



SCHOOL of
GRADUATE STUDIES
EAST TENNESSEE STATE UNIVERSITY

East Tennessee State University
Digital Commons @ East
Tennessee State University

Electronic Theses and Dissertations

Student Works

5-2010

An Active Study of a Roller Coaster Project in Asia.

Robert Leamon Bridges
East Tennessee State University

Follow this and additional works at: <https://dc.etsu.edu/etd>



Part of the [Operational Research Commons](#), and the [Risk Analysis Commons](#)

Recommended Citation

Bridges, Robert Leamon, "An Active Study of a Roller Coaster Project in Asia." (2010). *Electronic Theses and Dissertations*. Paper 1670.
<https://dc.etsu.edu/etd/1670>

This Thesis - Open Access is brought to you for free and open access by the Student Works at Digital Commons @ East Tennessee State University. It has been accepted for inclusion in Electronic Theses and Dissertations by an authorized administrator of Digital Commons @ East Tennessee State University. For more information, please contact digilib@etsu.edu.

A Study of a Roller Coaster Project in Asia

A thesis

presented to

the faculty of the Department of Business and Technology

East Tennessee State University

In partial fulfillment

of the requirements for the degree

Master of Science in Engineering Technology

by

Robert Leamon Bridges

May 2010

Dr. W. Andrew Clark, Chair

Dr. J. Paul Sims

Dr. Hugh K. Rogers

Dr. Keith V. Johnson

Keywords: Automated Ball Indentation test, nondestructive test, Stress-Strain Microprobe

TM, yield strength, ultimate tensile strength

ABSTRACT

An Active Study of a Roller Coaster Project in Asia

by

Robert Leamon Bridges

A roller coaster manufacturer became aware that improperly heat treated track couplings were sent to a construction site for assembly. Concerns were that suspect couplings might not meet the engineering specifications and could be vulnerable to sudden failure. A testing company in Oak Ridge, TN that specializes in in-situ and laboratory mechanical testing was contacted by the manufacturer for help in this endeavor. The construction company elected to enlist a local testing firm to perform field tests on the components instead of the company in Oak Ridge. The test methods used are incapable of providing quantitative results that could be measured to the engineering specifications, making it unlikely to identify anything but the worst material conditions. This study is an example that the need for accurate analysis is very important. The manufacturer reported that 60 couplings were replaced, but it is presently unknown how many should have been replaced.

Copyright © 2010 by Robert L. Bridges, All Rights Reserved

ACKNOWLEDGEMENTS

I wish to express a special thanks to Mr. Fahmy M. Haggag for his untiring effort to educate me in the science of mechanical testing and the use of his invention, the Stress-Strain Microprobe TM system and specifically the Automated Ball Indentation test. Mr. Haggag is truly a visionary and pioneer in the field of mechanical and fracture toughness testing.

CONTENTS

	Page
ABSTRACT.....	2
ACKNOWLEDGEMENTS.....	4
LIST OF TABLES.....	6
ACRONYMS, ABBREVIATIONS, AND INITIALISMS.....	9
Chapter	
1. INTRODUCTION.....	12
Problem Statement.....	15
ABI Summary Results.....	16
2. LITERATURE REVIEW.....	17
ABI Test.....	17
NDT Methodology.....	20
ABI Test Method.....	23
The SSM System and ABI Theory.....	28
Testing Procedure and Results.....	30
3. RECOMMENDATIONS FOR IMPROVEMENT.....	41
Define Phase.....	41
Measure Phase.....	41
Precision and Bias Statements – Interlaboratory Study Program.....	42
Analyze Phase.....	46
Improvement Phase.....	50
Control Phase.....	51
4. CONCLUSIONS.....	52
REFERENCES.....	53
APPENDIX: Article on the ABI Test.....	55
VITA.....	73

LIST OF TABLES

Table	Page
1. ABI Test Data for Two Weld Zones and the Base Metal Region	19
2. An Empirical Correlations Between Charpy Impact and Fracture Toughness Can Be Derived from the Following Table.....	34
3. A Summary of Tensile and Fracture Toughness Properties from the Steel Coupling Specimens.....	34
4. Details of the Fracture Toughness Calculation from ABI Tests on the Five Specimens...	38
5. Shows the CV% Data of the Most Common ABI-Measured Flow Properties from the ILS Program	43
6. A Precision Summary from the Yield Strength Measurements from the ILS Program.....	44
7. Is the Sample-Size Code Letters (Table 1 of ANSI/ASQ Z1.4)	45
8. Some Important Factors to Consider that Contribute to Nonconforming Units When Determining Quality Analysis.....	46
9. The Poisson Distribution for the Sampling Plan	48

LIST OF FIGURES

Figure	Page
1. Shows Roller Coaster Being Assembled Like the One in Asia	14
2. a Track Coupling is Shown, Consisting of Two Major Steel Castings, Similar to the Type Evaluated during the Study.....	14
3. Shown is a Digital Micrograph, Made Using Polarized Light, of a TIG Weld in Steel Showing the Different Weld Zones. The Three Indents (Round Circles) Were Made from ABI Tests.	18
4. Shows True-Stress/True-Plastic-Strain Curves of the Various Weld Zones from ABI Tests	19
5. <i>A and B.</i> Digital Microstructures from Specimens “A” and “B” at 50x Magnification ...	22
6. <i>6 C and D.</i> Digital Microstructures from Specimens “C” and “D” at 50x Magnification	22
7. <i>7E1 and 7E2.</i> More Martensite Can Be Seen in the Pearlite Dominant Microstructure than the Other Specimens. Specimen “E1” is Shown at 50x Magnification and “E2” at 500x Magnification.	22
8. SSM System Mounted on a Section of Steel Gas Pipeline Using Magnetic Mounts	30
9. A Graph Overlaying ABI Force versus Indentation Depth on the Five Samples.	35
10. A Graph Overlaying Five True-Stress versus True-Plastic-Stain Curves from the Five Specimens	36
11. The Fracture Toughness Master Curve of Specimen “E1”	36
12. Specimen “A” Satisfied the Critical Fracture Strain Model (2037 MPa) at Room Temperature	37
13. Specimen “E1” Satisfied the Critical Fracture Stress Model (2345 Mpa) at Room Temperature	37
14. Shows the Fracture Toughness Master Curve (K_{Jc} Vs. Temperature) from Triplicate ABI Tests Conducted on Specimens “C”, “D”, And “E1”. The T_0 Values are -9°C, -14°C, and 0°C, Respectively	39

LIST OF FIGURES CONTINUED

Figure	Page
15. Shows a Normalized Plot of the Fracture Toughness Master Curve from Triplicate ABI Tests Conducted on Specimens “C”, “D”, and “E1”. The Reference Temperature T_0 is the Temperature at a Median Fracture Toughness Level of 100 $\text{MPa}\sqrt{\text{M}}$	39
16. Shows the Cause-And-Effect “Fishbone” Diagram for Possible Contributors	46
17. Shows the SIPOC Process Chart for Using SSM to Measure Mechanical Properties.....	47
18. Shows the Manufacturers α Risk	49
19. Shows the Consumer β Risk	49
20. Shows the AOQ Curve That Includes the AOQL.....	50

ACRONYMS, ABBREVIATIONS, AND INITIALISMS

α	Alpha risk
ABI	Automated Ball Indentation
Ac	Acceptance number
ANSI/ASQ	American National Standards Institute - American Society of Quality
ASTM	American Society for Testing and Methods
ATC	Advanced Technology Corporation
AOQL	Average Outgoing Quality Limit
AQL	Average Quality Level
β	Beta risk
BHN	Brinell hardness number
c	acceptance number
C	Centigrade
C-LR	Circumferential primary direction – L and R are secondary directions
CTQ	Critical To Quality
CV	Coefficient of Variation
CVN	Charpy V-notch
dt/D	total indenter diameter during loading divided by the diameter of the indenter
E	Prefix for ASTM standard
ILS	Interlaboratory Study
in/s	inches per second
J	joule
K	Strength coefficient

K_{Jc}	Fracture toughness from J integral at the crack tip (from modified specimen)
K_{Ic}	Fracture toughness
L-CR	maximum grain flow primary direction – C and R are secondary directions
ln	natural logarithm
LQ	Limiting Quality
m	meters
MIL-STD	Military Standard
mm	millimeter
mm/s	millimeter per second
M.C.	Master Curve
MPa	Megapascal
$MPa\sqrt{m}$	Megapascal multiplied by meters square root or $MPa \cdot m^{1/2}$
n	Strain hardening exponent
N	Newton
n_2	Sample size
N_2	Lot size
NDT	Nondestructive Test
r	Repeatability within a laboratory
R	Repeatability between laboratories
R_c	Non-acceptance or reject number
R-LC	Radial primary direction – L and C are secondary directions
RQL	Rejection Quality Level
SSM	Stress-Strain Microprobe TM

SIPOC	Suppliers, Inputs, Processes, Outputs, Customers chart
STP	Standard Test Procedure
T ₀	Temperature, initial
UTS	Ultimate Tensile Strength
x	Magnification of an object multiplied by its original size
YS	Yield Strength

CHAPTER 1

INTRODUCTION

There are many destructive and a few nondestructive test (NDT) methods available for measuring mechanical properties for various applications. This study provides an example of how useful the correct NDT method is when used appropriately and how worthless, and potentially dangerous, the information is when using incorrect NDT methods.

In the summer of 2009 a roller coaster manufacturer became concerned about track coupling components that were improperly heat treated after casting and before being final machined, assembled, and shipped to a construction site in Asia for final assembly into a new roller coaster ride. The suspect components make up the couplings that connect and align the sections of track that the cars of the roller coaster ride on. Figure 1 shows the roller coaster track during assembly that looks similar to the one on the construction site in Asia. The manufacturer's concerns were that some of the components, similar to the one pictured in Figure 2, might be more brittle than the properly heat treated components and, therefore, vulnerable to sudden catastrophic failure. Advanced Technology Corporation (ATC) is a testing company in Oak Ridge, TN that specializes in destructive and nondestructive mechanical testing in both laboratory and field conditions and was contacted by the roller coaster manufacturer for help in identifying the suspect components. The construction company was not receptive to having ATC conduct field testing, but chose instead to use a testing firm closer to the construction site to field test the components. The NDT methods that were believed used were not appropriate for determining tensile and fracture measurements that the manufacturer requested. The NDT methods used included a handheld alloy analyzer (similar to the type used in metal scrap yards), and microstructure field

replicate system to determine if the heat treating was correctly executed. The specific NDT methods used are discussed further in the Methodology and Potential Causes section of this manuscript.

The manufacturer asked ATC to (1) nondestructively measure the tensile and fracture toughness properties of five steel specimens sectioned from coupling components and (2) identify components that did not meet Charpy impact energy equal to or less than 34J at -20°C. ATC's response was to use the Automated Ball Indentation (ABI) test to (1) nondestructively measure the tensile and fracture toughness properties of five steel specimens, four from tested Charpy V-Notch (CVN) specimens and one from a coupling segment, all of the specimen were sectioned from coupling components and (2) identify components that did not meet Charpy impact energy equal to or less than 34J at -20°C with some stipulations. Besides measuring tensile properties, ABI is used to measure the fracture toughness (K_{Jc}) of steels (for details see section on ABI Test Method) and comparisons can be made between CVN impact energy and fracture toughness in the transition region based on empirical correlation. (Rolfe & Novak, 1970) ABI can measure fracture toughness in field applications; however, it is impractical to field test components at -20°C and fracture toughness (K_{Jc}) is not the same measurement as a CVN fracture test. An empirical correlation was made between the Charpy impact energy and fracture toughness measurements. To validate this correlation fracture measurement comparisons had to be verified. The manufacturer's engineering specification of 34J impact energy at -20°C is equivalent to a fracture toughness value of 95 MPa \sqrt{m} at -20°C and a critical fracture stress value of 3300MPa. Because field testing would have to be conducted at ambient temperature instead of -20°C, the critical fracture stress used to analyze the ABI data was

adjusted from 3300MPa to 2345 MPa, using the Fracture Toughness Master Curve concept of ASTM standard E1921.



Figure 1. Shows Roller Coaster Being Assembled Like the One in Asia



Figure 2. A Track Coupling is Shown, Consisting of Two Major Steel Castings and Similar to the Type Evaluated during the Study

Problem Statement

Within a roller coaster ride recently constructed in Asia there are 450 track couplings consisting of two heat treated components making up each coupling, for a total of 900 components. Some of them may be outside the engineering fracture requirements established by the manufacturer due to inadequate heat treatment of some of the components. There was a construction deadline looming (at the time of the request) so in order to successfully field test 100% of every coupling component on the ride it would take a crew of three up to 10 days to perform triplicate ABI tests on all 900 components and provide a summary report of the 2,700 test results and identify the substandard components to the construction contractor and the manufacturer. The concern that the construction company used an inferior NDT method and therefore, make it impossible of knowing how many components are actually outside the fracture specification. However, the risk of not meeting the construction deadline will undoubtedly be avoided by this practice. What is the potential cost of not properly identifying and replacing suspicious components? The cost of inspecting 900 components is approximately \$860,000 based on the pricing information from ATC's accounting record proposals. The probability of a roller coaster failure or ride accident is above the acceptable risk according to safer park, which summarizes that general product liability insurance for roller coaster parts manufacturers is up to \$1,000,000 per claim or \$2,000,000 aggregate (General product liability, 2009). The cost of \$860,000 for 100% inspection of 900 components for the removal of defective components will reduce the probability of equipment or part failure in terms of monetary damage and therefore cost savings in millions of dollars per accident/incident could be avoided.

Feedback ATC received from the manufacturer reported that the field testing conducted at the construction site identified 60 components that did not having the acceptable microstructure and were replaced. The manufacturer did not comment whether all of the components had been inspected or if there were plans to systematically replace the remaining couplings.

ABI Summary Results

To summarize the ABI test results in Table 3 at measuring the mechanical behavior, i.e. yield strength (YS), ultimate tensile strength (UTS), and fracture toughness values of the five steel specimens show that “A” and “B” are very similar and specimens “C” and “D” are also similar. Specimens “C” and “D” have mechanical properties similar to specimen “E1”. It should be noted that specimen “E1” was machined from a broken coupling segment and not a CVN specimen, like “A – D”. In order to verify that orientation was not an issue for measuring mechanical properties, because the orientation of the CVN specimens were unknown, specimen “E” was tested on three primary axes. The axial alignment of the ABI indenter during the tests on specimen “E” were; circumferential primary direction (C-LR), maximum grain flow primary direction (L-CR), and radial primary direction (R-LC).

To be specific, of the five specimens tested only specimens “A” and “B” met the manufacturer’s engineering (fracture mechanics) criteria and specimens “C”, “D”, and “E1” are considered unacceptable. The details of the ABI test results are provided in the Testing Procedure and Results section.

CHAPTER 2

LITERATURE REVIEW

ABI Test

ATC specializes in laboratory and field testing of various metallic materials, but they predominantly do field testing of pipeline steel. Since 1989 the principle investigator been interested in the Stress-Strain Microprobe™ (SSM) system as a means of collecting baseline mechanical properties without having to section components and to be able to use the same equipment as an alternative to traditional destructive testing, i.e. tensile and fracture toughness testing. The ABI test method is used for nondestructive mechanical property measurements. The ABI test has two significant advantages over the destructive testing of specimens; being localized and requires no machined test specimen. The ABI test, developed by ATC, is a direct measurement of mechanical properties and is considered a NDT because it does not remove material and leaves a smooth spherical depression with no sharp edges or stress-concentration sites. Theory and details on how ABI works are in the ABI theory and Appendix sections of this manuscript.

The ABI test was first developed in mid 1980s and was used in the late 1980s to measure the neutron embrittlement effects on ferritic steels (Haggag, 1989). Typically, ABI is used to measure subtle differences in the mechanical behavior between areas of a sample or between different samples. Common requests include the nondestructive comparison of the mechanical behavior across a welded section and to determine if a sample meets a desired heat treat condition. Figure 3 shows a digital photomicrograph of a weld under polarized light and Figure 4 is the true-stress versus true-plastic-strain curves from ABI used to measure the mechanical properties across the weld.

Table 1 is a summary of the yield strength, tensile strength, and Brinell hardness at each zone of a steel tungsten inert gas (TIG) weld. The base metal region is very fine equiaxed grains; the heat affected zone has slightly larger grains with almost a halo effect around the weld pool or fusion zone. The fusion zone is where the actual molten metal directionally solidified after the weld into very large columnar (elongated, column-like) grains.

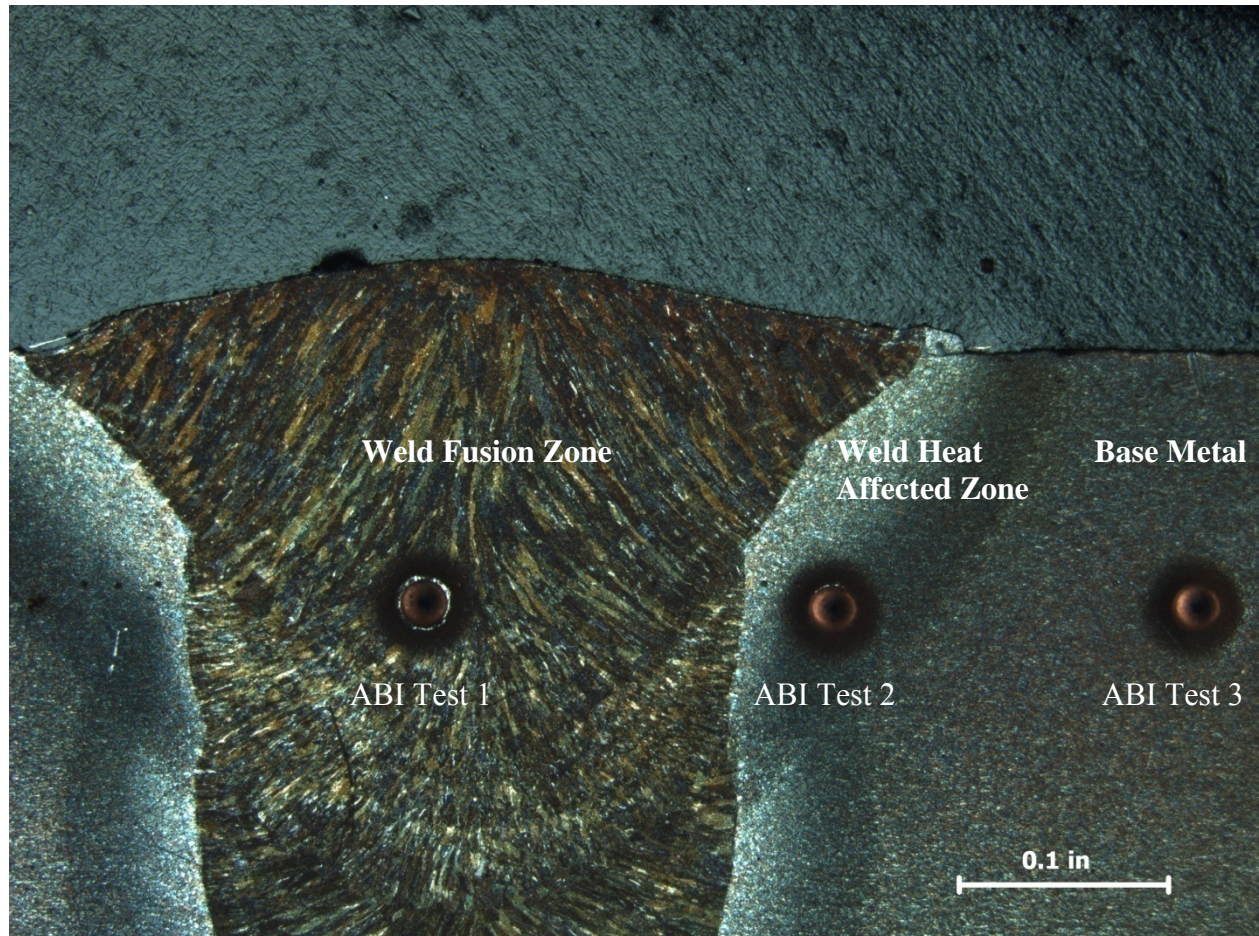


Figure 3. Shown is a Digital Micrograph, Made Using Polarized Light, of a TIG Weld in Steel Showing the Different Weld Zones. The Three Indents (Round Circles) Were Made from ABI Tests.

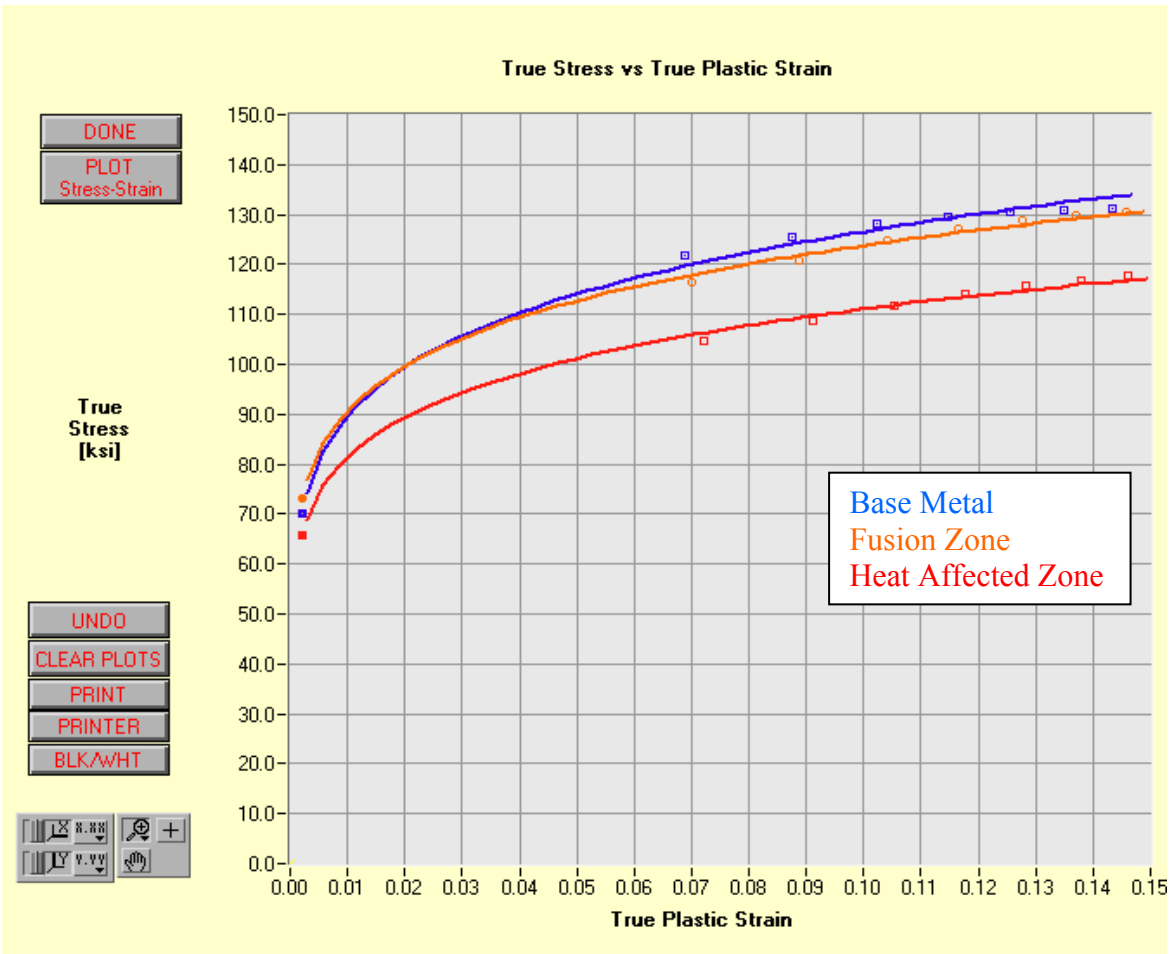


Figure 4. Shows True-Stress/True-Plastic-Strain Curves of the Various Weld Zones from ABI Tests

Table 1.

ABI Test Data for Two Weld Zones and the Base Metal Region

TIG Welded Steel, ABI Test Data			
Test date: April 03, 2008			
Test temperature (F): 75			
Indenter speed (in/in/sec): 0.001			
Indenter diameter (in): 0.03			
Test Name	Yield Strength, (n,K)[ksi]	Calculated Engineering UTS [ksi]	Brinell Hardness Number (BHN)
Base Metal	70.4	115.4	252
Fusion Zone	73.0	112.6	260
Heat Affected Zone	65.5	101.1	233
Standard Deviation	3.8	7.6	13.9

Doing the same measurements with conventional tensile tests is difficult or impossible and requires destroying a section of the component in order to make multiple test specimens.

NDT Methodology

The NDT methodology the construction company chose to determine the quality of the track couplings consisted of using silicone replicates of the microstructure and portable alloy analyzers. Silicone replicates are NDT methods recognized by ASTM, E1351-01 Standard Practice for Production and Evaluation of Field Metallographic Replicas (E1351-01, 2006), but portable analyzers are not. However, these NDT methods are not suitable for this application.

The components that make up a coupling are cast, heated to very high temperatures, and quenched quickly (rapidly cooled in water or similar medium) to retain a specific microstructure. The suspect material appears to have been quenched very quickly and therefore shows retained martensite (“needle-like” structure) in the dominantly pearlite (darker regions) microstructure, which can be brittle in low carbon steels at very low temperatures. Figures 5A, 5B, 6C, 6D, 7E1, and 7E2 show the digital optical micrographs made from the five specimens. There are some observable differences in the proportions of ferrite (light regions) and pearlite (dark regions) in the microstructures between specimens “A” and “B” and “C” and “D”, but there is a noticeable difference in the amount of pearlite with martensite in the microstructure between specimen “E1” and the other four specimen. Specimen “E2” is actually the same area as “E1” at a higher magnification. One could conclude that the suspect material, such as specimen “E1”, could be identified optically at modestly low magnification (such as 50x). However, it should be understood that from the ABI test results only specimen “A” and “B” met engineering design expectations and the

other three specimens did not. Therefore, doing field replicates to detect subtle differences between the first four microstructures would be difficult under laboratory conditions and nearly impossible from replicates collected in the field from coupling components that were already assembled between track sections. All of the digital optical micrographs in figures 5A, 5B, 6C, 6D, 7E1, and 7E2 were made from metallography specimens prepared in our metallography laboratory.

A replicate is a fast curing, two-part silicone rubber that is designed to transfer the structure of a solid surface. The result is a three-dimensional copy of the surface, allowing metallographic examination. The replicate can provide highly accurate detail down to 0.1 micron. However, grinding and polishing 900 coupling components in the field and using replicates to determine which components were properly heat treated is not practical or realistic.

The handheld alloy analyzer is a portable spectrometer, either X-ray fluorescence or spark-source optical emission. These relatively inexpensive spectrometers are typically used in metal scrap yards to segregate various metals and alloys. Some high-end models can measure carbon and other constituents to parts per million. Without a doubt, most alloy analyzers can identify one type of steel from another; however, the pedigree of the steel components were made from was not in question, the mechanical characteristics were. Alloy analyzers cannot determine the heat treatment or mechanical behavior of the metal being tested. There is an ASTM test standard for determining ferrite and austenite phases in steels, E 975-03 X-ray Determination of Retained Austenite in Steel with Near Random Crystallographic Orientation, but it is a destructive test and cannot differentiate ferrite from martensite (E975-03, 2008).

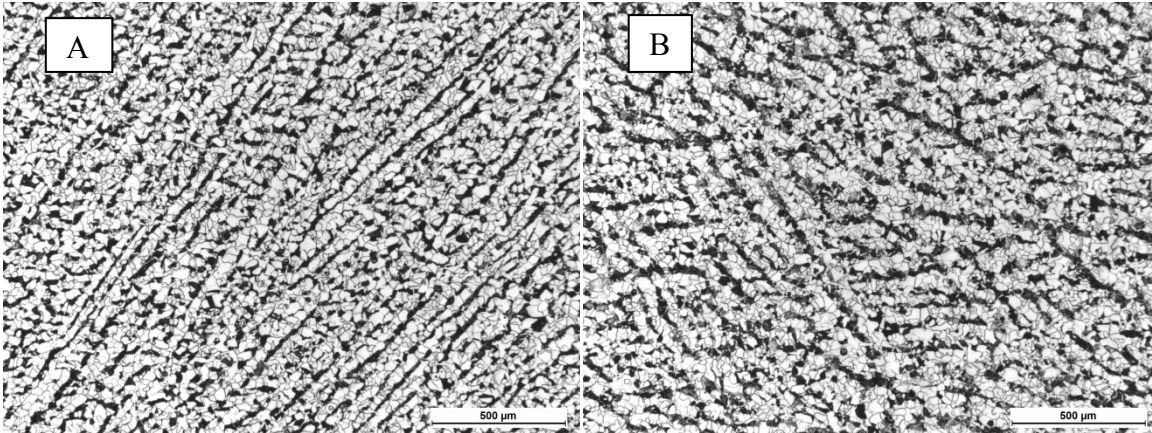


Figure 5A and B. Digital Microstructures from Specimens “A” and “B” at 50x Magnification

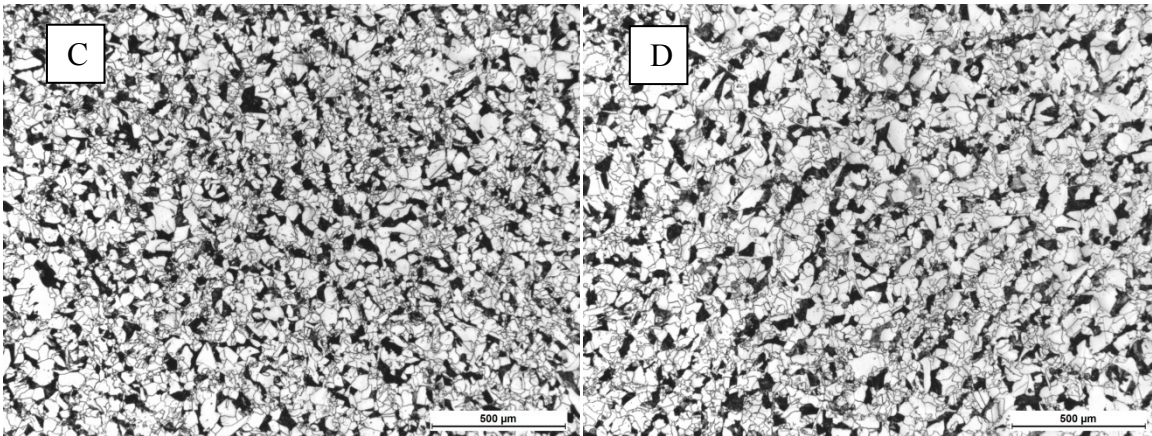


Figure 6 C and D. Digital Microstructures from Specimens “C” and “D” at 50x Magnification

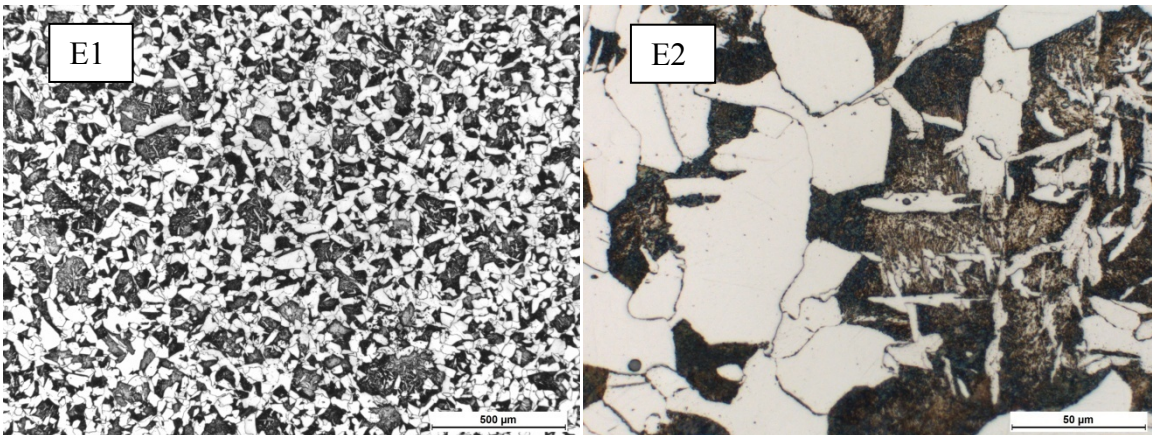


Figure 7E1 and 7E2. More Martensite Can Be Seen in the Pearlite Dominant Microstructure than the Other Specimens. Specimen “E1” is Shown at 50x Magnification and “E2” at 500x Magnification.

ABI Test Method

In order to understand the ABI test it is important to appreciate the aspects of the test and what the data represent. As mentioned before, the ABI test is a NDT method that provides mechanical property data using a spherical indenter, usually made from tungsten carbide. The indenter is forced into the specimen surface and at several predetermined intervals the indenter is allowed to partially unload, followed by additional loading until a set amount of the total diameter of the indenter has been pressed into the surface, typically between 10% – 40% of the spherical diameter of the indenter. Figure 8 shows what a typical force versus depth graph looks like after several tests. The ABI test can only provide data to about 20%, or less, of the stress-strain curve relying on estimation or calculations using n and K to determine the UTS and assuming the material stress-strain curve follows a power law. After the ABI test is completed the results are analyzed and the data can be represented by several different charts like the ones in Figures 9, 10, and 11 or by report summary as in Tables 3 and 4. The SSM can perform traditional (destructive) tensile or fracture toughness tests and the data can be overlaid with the ABI results for visual comparison. For comparison sake the ABI tests can be performed on the tensile or fracture toughness test specimen prior to being destructively tested.

Before testing the SSM is allowed to warm up and an internal shunt resistor is checked during this phase to insure that the load cell reading is the same as the value recorded in the certification documents. It is always good to test the system on a blank prior to actual testing to insure everything is working properly. This pretest can be performed on a test block of a similar metal if desired to assure that preload and load ranges are appropriate. The typical ABI test takes between 2 and 3 minutes to run depending on the test speed

selected. Analyzing the test results and creating a new file name for the next test takes about 1 minute; therefore, in less than 5 minutes the mechanical properties of a metal specimen can be determined without the need of a machined specimen.

The ABI test gives the following measurements:

1. Yield strength
2. Strength coefficient (K) - Strain hardening exponent (n)
3. Engineering ultimate tensile strength
4. Percent uniform ductility
5. Brinell hardness by ABI
6. Fracture toughness
7. Critical stress
8. Critical depth

The following definitions are from my understanding of the terms from experience, along with perhaps more precise definitions found in ASM Materials Engineering Dictionary (Davis, 1992).

1. Yield strength is the transition from elastic to plastic deformation and is usually observed as an abrupt change on an engineering stress-strain curve. The material can no longer recover to its original shape after it has reached its yield point. Yield strength is measured in stress (force per unit area) in either ksi or MPa units. “The stress at which a material exhibits a specified deviation from proportionality of stress and strain. An offset of 0.2% is used for many materials, particularly metals.” (Davis, 1992). “Yield strength, σ_{YS} – the stress at which a material exhibits a specific limiting deviation from proportionality of stress to strain at the test temperature. This

deviation is expressed in terms of strain.” ASTM International, E1823-09a (E1823-09a, 2009).

2. Strength coefficient (K) and strain hardening exponent (n) are used in conjunction to determine the ability of a given material to be formed. Typically the higher the n-value the more easily it can be formed. “The value of n in the relationship:

Equation 1

$$\sigma = K\varepsilon^n \text{ units in SI or English}$$

Where σ is the *true stress*, ε is the *true strain*, and K, which is called the strength coefficient, is equal to the true stress at a true strain of 1.0. The strain-hardening exponent, also called “ n -value,” is equal to the slope of the true stress versus true strain curve up to maximum load when plotted on log-log coordinates. The n -value relates to the ability of a sheet material to be stretched in metalworking operations. The higher the n -value, the better the formability (stretch-ability)” (Davis, 1992).

3. Engineering ultimate tensile strength is the point at which a material being pulled in tension can no longer deform before it breaks. The ABI test does not test to failure; therefore, this value is determined by the shape of the true-stress / true-plastic-strain curve. UTS is measured in stress (force per unit area) in either ksi or MPa units. “The ultimate or final (highest) stress sustained by a specimen in a tensile test” (Davis, 1992).
4. The percent of uniform ductility is the amount stretching a material can undergo in tension before necking occurs along the gage section of a tensile specimen. “Uniform elongation. The elongation at maximum load immediately preceding the onset of necking in a tensile test” (Davis, 1992).

5. Brinell hardness by ABI is measured the same way as a Brinell hardness test except with a spherical indenter less than the typical 10mm diameter, usually a 0.254, 0.508, 0.762 or 1.575-mm spherical indenter. It is used to show comparative hardness from one test to the next. “A test for determining the hardness of a material by forcing a hard steel or carbide ball of specified diameter (typically 10mm) into it under a specified load. The result is expressed as the *Brinell hardness number*.” (Davis, 1992)
6. Fracture toughness is the resistance of a material to extend a crack during deformation, usually during cyclic tensile loading. It does not initiate the crack, but it is the amount of stress necessary to cause the crack to extend (lengthen). Fracture toughness is identified as K_{IC} or for smaller specimen geometry K_{JC} typically and measured in $MPa\sqrt{m}$ or $MPa\cdot m^{0.5}$ units. “A generic term for measures of resistance to extension of a crack. The term is sometimes restricted to results of *fracture mechanics* tests, which are directly applicable in fracture control. However, the term commonly includes results from simple tests of notched or pre-cracked specimens not based on fracture mechanics analysis. Results from tests of the latter type are often useful for fracture control, based on either service experience or empirical correlations with fracture mechanics tests” (Davis, 1992).
7. Critical stress is the critical fracture stress value that a material is expected to resist before crack extension. “Stress-intensity factor. A scaling factor, usually denoted by the symbol K , used in *linear-elastic fracture mechanics* to describe the intensification of applied stress at the tip of a crack of known size and shape. At the

onset of rapid crack propagation in any structure containing a crack, the factor is called the critical stress-intensity factor, or the *fracture toughness*” (Davis, 1992).

8. Critical depth is how far the indenter is forced into the surface of a material to measure the critical stress. No definition available found in ASM Materials Engineering Dictionary.

While performing and analyzing ABI results it is important to understand the information that is the most pertinent for the intended application. For example, if the interest is in formability, then values for K, n, and perhaps percent uniform ductility are more valuable than UTS or fracture toughness. However, if the intent is like the one in this study, then yield strength UTS and fracture toughness are paramount, which are highlighted in Table 3. Although the customer was only interested in comparison between fracture toughness and CVN results, the comparative differences in the lot of specimens was apparent from BHN in Table 3 and the graphs in Figures 8 and 9.

The CVN test is a fairly simple test where a machined rectangular specimen, typically measuring 10-mm by 10-mm by 55-mm, is made with a machined V shaped notch across the central length. A hammer attached to a pendulum strikes the fixed specimen from the side opposite the V-notch and the force needed to fracture the specimen is recorded. The fracture measurement comes from measuring the height that the hammer would travel without striking the specimen compared to the height it travels after striking the specimen. There is a great deal of variation in the recorded CVN fracture data typically and, therefore, a lot of specimen must be tested before a baseline can be determined.

The SSM System and ABI Theory

Some of the theoretical development behind the ABI test is well characterized in the open literature by Tabor (1951) in the early '50s and several engineering application studies involving its use have been documented mostly by Haggag (1989) and some by Byun, T. S., Hong J. H., Haggag F. M. & Lee E. H. (1997) in recent years. For nearly 60 years Tabor (1951) studied the relationship between ball indentation measurements and true stress versus strain curves similar to tensile properties of work hardened metals. Later, Haggag (1989) invented the ABI test technique and developed the SSM to measure mechanical data using some of the equations from Tabor (1951) and some new empirical relationships. The ABI test is a multi-axial test, not a tensile test, even though it provides similar values. The ABI test relies on multiple cyclic loadings and innovative partial unloadings of a spherical tungsten carbide or silicon nitride ball indenter into the surface of the metal being tested. Because deformation of the specimen occurs during the loading cycles, the ABI software records the elastic plastic behavior during deformation. In an ABI test the deformation volume is not constant (like in a tensile test) but continually increases with increasing ball indentation depth. Hence, yielding and work-hardening occur simultaneously during the entire ABI test. The yield strength is calculated from all ABI loading cycles. From the true stress versus true plastic strain curve generated during the test analysis both estimated and calculated ultimate tensile strength values are determined. There is no necking element of the ABI test; therefore, UTS is more of a prediction based on power law principles instead of a necking point, as from a tensile test.

A summary of the ABI technique is given with more details in some of Mr. Haggag's papers in the Appendix section "In-Service Nondestructive Measurements of

Stress-Strain Curves and Fracture Toughness of Oil and Gas Pipelines: Examples of Fitness-for-Purpose Applications" (Haggag, 2002). The SSM system can be configured for ABI field and laboratory testing as well as for testing of miniature tensile test specimens. The ABI technique is based on strain-controlled multiple indentations (at a single penetration location) of a smooth surface by a nonlinear-geometry indenter (tungsten carbide spherical indenters of 0.01 to 0.062-inch diameter). The indentation depth is progressively increased to a maximum user-specified limit with innovative intermediate partial unloading of the indenter during the ABI test. The applied indentation loads and associated penetration depths are continuously acquired during the ABI test and used to calculate the incremental stress-strain values based on elasticity and plasticity theories and a few empirically based equations.

The microprobe system uses an electromechanically driven indenter, high-resolution penetration transducer and load cell, a personal computer (PC), a 16-bit data acquisition and control unit, and copyrighted ABI software. Results of ABI tests on various base metals, weld, and HAZs at different metallurgical conditions are presented and discussed in this manuscript. Excellent agreement was obtained between ABI-derived data and those data from conventional American Society for Testing and Materials (ASTM) test methods.

ATC successfully tests steel pipe by both magnetic and clamp-mounted SSM configurations as shown in Figure 8. Part of measuring the mechanical properties of pipe includes both girth and seam welds when applicable. Yield strength and flow property measurements usually follow changes in material microstructure. For example, in a weld where there are distinct changes in the microstructure between the heat affected zone, fusion

zone and base metal areas as illustrated in the TIG weld shown in Figures 3 and 4, typical of pipeline welded steel.



Figure 8. SSM System Mounted on a Section of Steel Gas Pipeline Using Magnetic Mounts

Testing Procedure and Results

Three ABI tests were conducted on each of four broken CVN specimens and nine tests were conducted on specimen “E1” (triplicates on three perpendicular faces) of the roller coaster steel segments received from the manufacturer, for a total of 21 ABI tests. All ABI tests were performed using a 0.762-mm (0.030-inch) diameter tungsten carbide indenter at an indenter speed of 0.02 mm/s (0.0006-in/s). The tensile and fracture toughness properties were determined from each ABI test. Table 3 is a summary of the ABI-measured tensile and fracture toughness properties for the 21ABI tests. In order to see if orientation has any effect on the ABI test data nine ABI tests were conducted in triplicates in three orientations of R-

LC, C-LR, and L-CR of specimen “E1” resulting in negligible effects (see Table 3 and Figures 9 and 10). For Specimen “E1” the nomenclature for the orientations, L = axial direction, R = radial direction, and C = circumferential or tangential direction, comes from ASTM E1823-09a and represent the primary indenter orientation to the surface the ABI test are performed. Graphs showing several curves of indentation force-depth data, and true-stress versus true-plastic-strain can be seen in Figure 9, and the three representative levels of strength and fracture toughness are shown in Figure 10. The graphs in Figures 9 and 10 show that there are two distinct lots of material having similar mechanical properties, specimens “A” and “B” are in one lot and specimens “C,” “D”, and “E1” in another. The five specimens measured distinct differences in tensile, fracture toughness properties, and Brinell Hardness Number (BHN) values. Specimens “A” and “B” did not meet the critical fracture stress model of the ABI test before reaching 12% strain, so the fracture toughness values were calculated based on the ductile critical fracture strain model at 12% strain. This enabled specimens “A”, and “B” to meet the acceptable fracture toughness values. Specimens “C”, “D”, and “E1” met the critical fracture stress of 2345MPa before reaching 12%; therefore, these specimens were analyzed using the critical fracture stress model of the ABI test and the Fracture Toughness Master Curve concept of ASTM Standard (E1921-09a, 2009). This information was then used to determine reference temperatures and calculate the median fracture toughness values at -20°C for these specimens. Using the ABI-determined three reference temperatures for specimens “C”, “D”, and “E1” (-9°C, -14°C and 0°C, respectively), the median fracture toughness values at -20°C are 87, 92 and 78 MPa√m, respectively (see Figure 12). Because all three of these values are below 95MPa√m then all three are considered unacceptable.

To determine which material can be considered acceptable material from the unacceptable material an empirical correlation was required to convert the manufacturer's acceptance criterion of 34J impact energy at -20°C to a fracture toughness criterion (K_{Ic} in $\text{MPa}\sqrt{\text{m}}$) because the ABI test measures fracture toughness and not impact energy. There is no CVN to K_{Ic} correlation available in literature for the upper shelf except for very high yield strength materials ranging from 760 to 1700 MPa) as shown at the top of Table 2. There are several correlations for the transition region depending on the ranges of yield strength and impact energy. Therefore, the appropriate correlation used from Table 2 for the roller coaster material is:

Equation 2

$$K_{Ic}^2 / E = 0.22(\text{CVN})^{1.5} \text{ for SI units}$$

This is the empirical correlation published in ASTM STP 463 and printed on page 344 of Hertzberg's text book (see Table 1) (Rolfe & Novak, 1970).

Using this equation with the manufacturer's acceptance criterion of CVN impact energy of 34J at -20°C the calculated K_{Ic} value is $95 \text{ MPa}\sqrt{\text{m}}$.

All ABI tests were conducted at room temperature; therefore, the critical fracture stress was determined (by iteration) so the ABI-determined fracture toughness master curve produces a median value at -20°C that is lower than that corresponding to a CVN value of 26J (slightly lower than the 29J of specimen "E1" (with 29J at $+20^{\circ}\text{C}$ and no test data at -20°C)). The critical fracture stress value of 2345 MPa produces the fracture toughness master curve shown in Figure 6 for specimen "E1". Also, examples of using the critical fracture strain model and the critical fracture stress model are shown in Figures 10 and 11. Details of the fracture toughness calculations of all 15 ABI tests are given in Table 3.

Specimens “A” and “B” satisfied the critical fracture strain model while specimens “C”, “D”, and “E1” satisfied the critical fracture stress model. The fracture toughness master curves for specimens “C”, “D”, and “E1” are given in Figures 13 and 14. It should be implicit that the fracture toughness master curve is applied only to test results satisfying the critical fracture stress model and that according to ASTM Standard E1921, materials with reference temperatures within 20°C are considered equivalent.

The ABI tests on specimens “C”, “D”, and “E1,” shown in Figures 13 and 14, correlated with reference temperatures of - 9°C, -14°C, and 0°C, respectively, which produce median fracture toughness values of 87, 91, and 78 MPa√m , respectively, which are below the acceptance value of 95 MPa√m. Because all of these values are within 20°C they should be considered one material and, therefore, unacceptable per the equivalent K_{Jc} criterion. Specimens “A” and “B” were analyzed according to the critical strain model because the critical fracture stress of 2345MPa was not reached at the critical depth of $d_i/D=0.6$ (strain = 12%), while specimens “C”, “D”, and “E1” were analyzed according to the critical fracture stress model because a maximum stress of 2345MPa was reached at a critical depth of less than 12% strain. The critical fracture stress value of 2345 MPa was calculated based on the ABI results of specimen “E1” where the median fracture toughness at -20C of 78MPa√m is equivalent to a Charpy impact energy of 26J which is lower than the 29J of specimen “E1” at ambient temperature.

Table 2.

An Empirical Correlations Between Charpy Impact and Fracture Toughness Can Be Derived from the Following Table.

Material	Notch	Test	Temperature Range	Range of Charpy Results(J)	σ_y (MPa)	Correlation	Ref.
A517D 4147 HY130 4130 12Ni-5Cr-3Mo 18Ni-8Co-3Mo	V-Notch	Impact	Upper Shelf	31 – 121 (23 – 89 ft-lb)	750 – 1700 (110 – 246 ksi)	$K_{IC}^2/\sigma_y = 0.64(CVN/\sigma - 0.01)$ $[K_{IC}^2/\sigma_y = 5(CVN/\sigma - 0.05)]$	14, 18
A517F A3202B ABS-C HY-130 18Ni(250) Ni-Cr-Mo-V Cr-Mo-V Ni-Mo-V	V-Notch	Impact	Transition	4 – 82 (3 – 60 ft-lb)	270 – 1700 (39 – 246 ksi)	$K_{IC}^2/E = 0.22(CVN)^{1.5}$ $[K_{IC}^2/E = 2(CVN)^{1.5}]$	18
A533B A517F A542	V-Notch	Impact	Transition	7 – 68 (5 – 50 ft-lb)	410 – 480 (60 – 70 ksi)	$K_{IC} = 14.6(CVN)^{0.5}$ $[K_{IC} = 15.5(CVN)^{0.5}]$	19

*This Table was Re-Typed For Clarity from Table 9.3 of the Reference: Hertzberg, Richard W., Deformation and Fracture Mechanics of Engineering Materials, 2nd Ed., (New York: John Wiley And Sons, 1983) Pages 344-345.

Table 3.

A Summary of Tensile and Fracture Toughness Properties from the Steel Coupling Specimens

Test Name	Yield Strength [MPa]	Strength Coeff. (K) [MPa]	Strain Hardening Exponent (n)	Estimated Engr UTS [MPa]	Calculated Engr. UTS [MPa]	Calculated Uniform Ductility [%]	ABI Hardness	Fracture Toughness [MPa*m ^{0.5}]
Specimen A								
A-L-RT-1	317	731	0.134	488	489	14.4	168	203
A-L-RT-2	322	712	0.128	481	482	14.3	167	201
A-L-RT-3	318	726	0.132	486	487	14.3	169	200
Average	319	723	0.131	485	486	14.3	168	201
St. Dev.	3	10	0.003	4	4	0.1	1	1
Specimen B								
B-L-RT-1	319	729	0.133	488	489	14.3	168	200
B-L-RT-2	325	749	0.134	501	501	14.5	172	205
B-L-RT-3	329	726	0.128	491	492	14.3	171	203
Average	324	735	0.132	493	494	14.4	170	203
St. Dev.	5	13	0.003	7	6	0.1	2.1	3
Specimen C								
C-L-RT-1	375	884	0.137	586	587	14.2	199	181
C-L-RT-2	383	884	0.135	590	591	14.2	202	168
C-L-RT-3	380	916	0.141	604	605	14.2	204	144
Average	379	895	0.138	593	594	14.2	202	164
St. Dev.	4	18	0.003	9	9	0.0	2.5	18
Specimen D								
D-L-RT-1	374	893	0.139	590	591	14.2	199	171
D-L-RT-2	382	866	0.132	581	582	14.2	199	182
D-L-RT-3	373	876	0.137	582	582	14.3	198	180
Average	376	878	0.136	584	585	14.2	199	178
St. Dev.	5	14	0.004	5	5	0.1	0.6	6

Specimen E1, R-LC Orientation								
E1-R-LC-RT-1	409	944	0.135	630	630	14.2	215	128
E1-R-LC-RT-2	410	892	0.126	606	606	14.2	211	156
E1-R-LC-RT-3	411	913	0.129	616	617	14.2	211	143
Average	410	916	0.130	617	618	14.2	212	142
St. Dev.	1	26	0.005	12	12	0.0	2.3	14
Specimen E1, C-LR Orientation								
E1-C-LR-RT-1	400	887	0.129	599	600	14.2	208	156
E1-C-LR-RT-2	409	924	0.131	620	621	14.1	214	134
E1-C-LR-RT-3	399	911	0.133	610	610	14.2	210	144
Average	403	907	0.131	610	610	14.2	211	145
St. Dev.	6	19	0.002	11	11	0.1	3.1	11
Specimen E1, L-CR Orientation								
E1-L-CR-RT-1	409	901	0.128	610	610	14.1	212	148
E1-L-CR-RT-2	412	924	0.130	622	622	14.2	214	133
E1-L-CR-RT-3	411	919	0.130	619	620	14.2	214	137
Average	411	915	0.129	617	617	14.2	213	139
St. Dev.	2	12	0.001	6	6	0.1	1.2	8

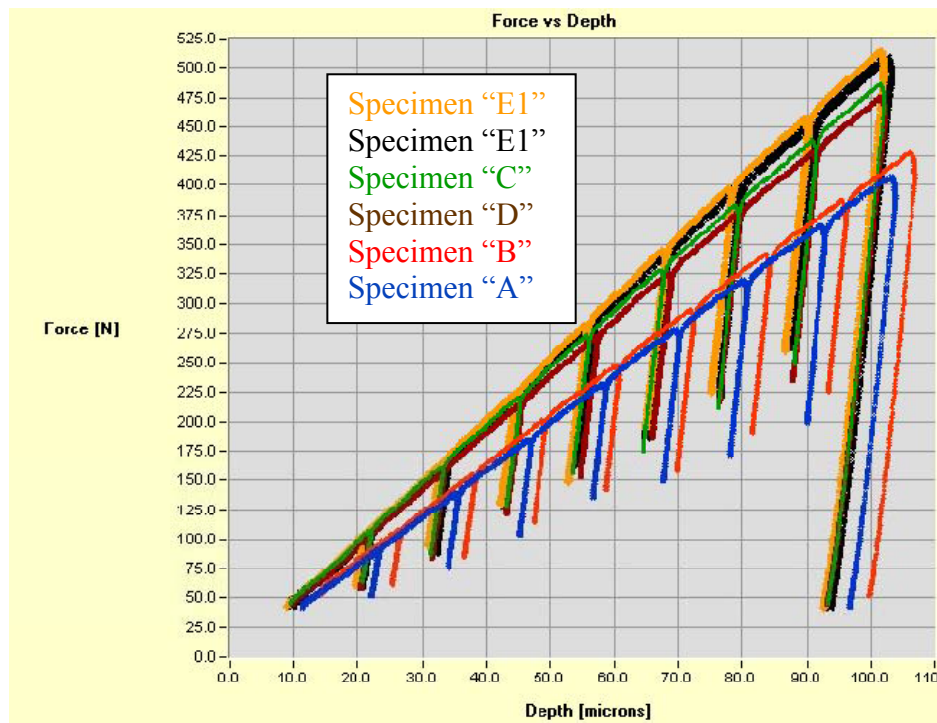


Figure 9. A Graph Overlaying ABI Force versus Indentation Depth on the Five Samples.
 - Note, E1 Was Tested Two Times

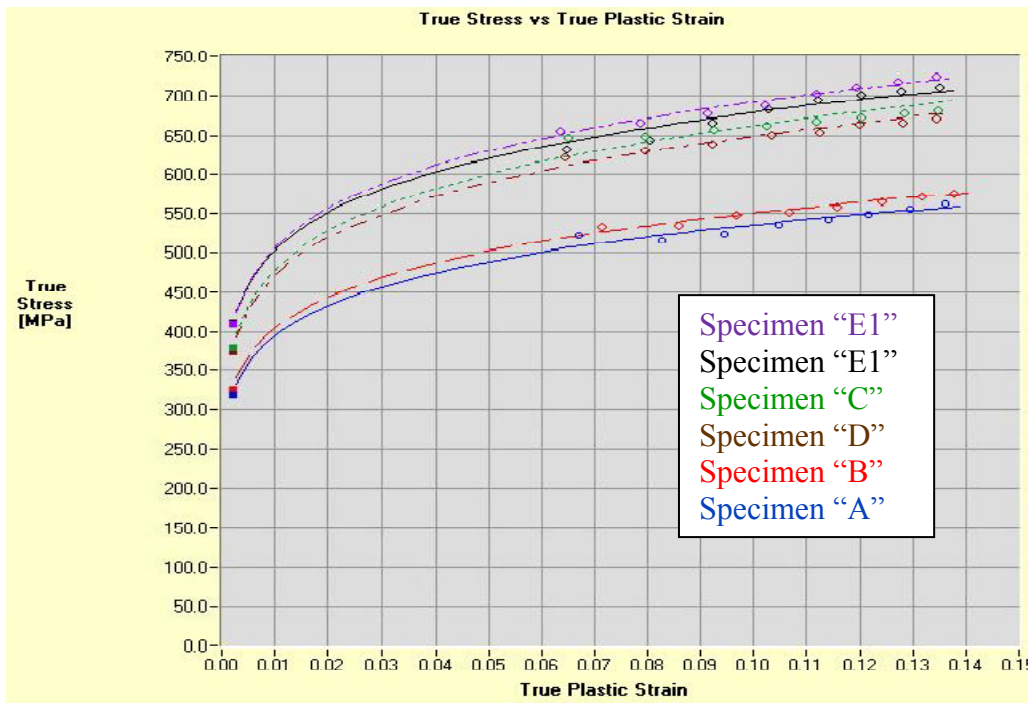


Figure 10. A Graph Overlaying Five True-Stress versus True-Plastic-Strain Curves from the Five Specimens

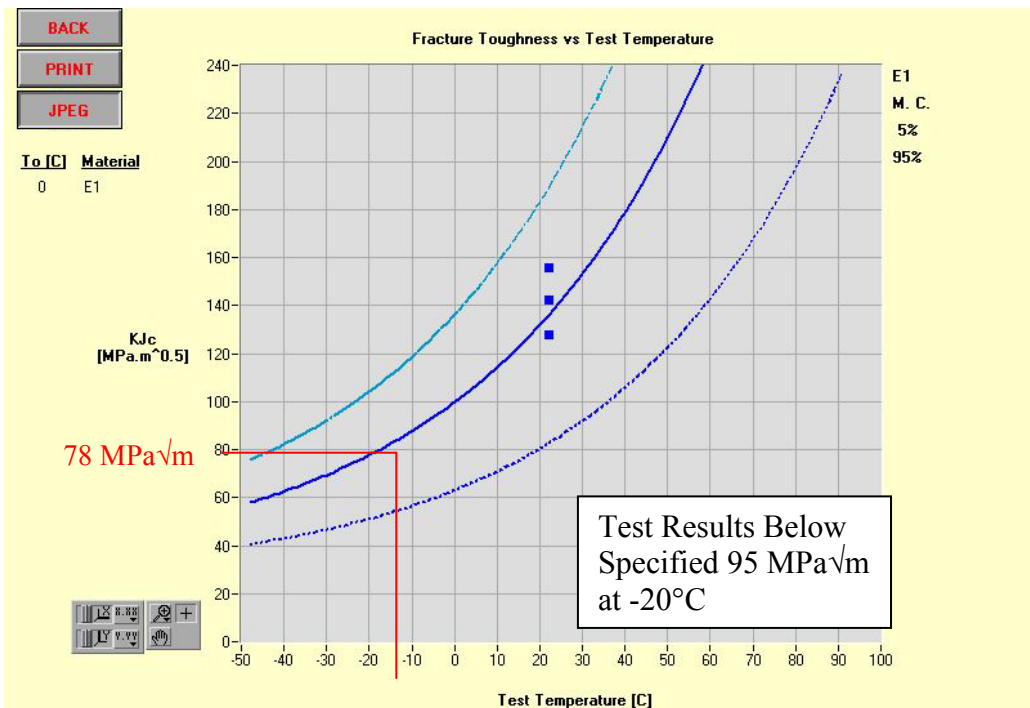


Figure 11. The Fracture Toughness Master Curve of Specimen "E1"

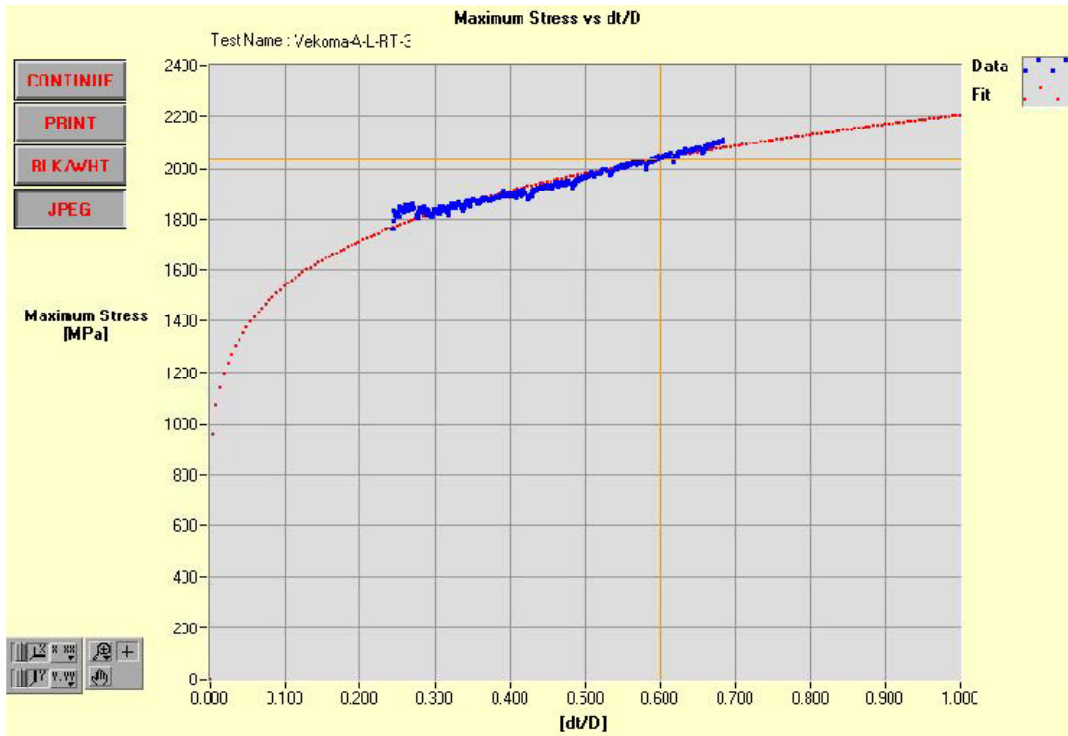


Figure 12. Specimen “A” Satisfied the Critical Fracture Strain Model (2037 MPa) at Room Temperature

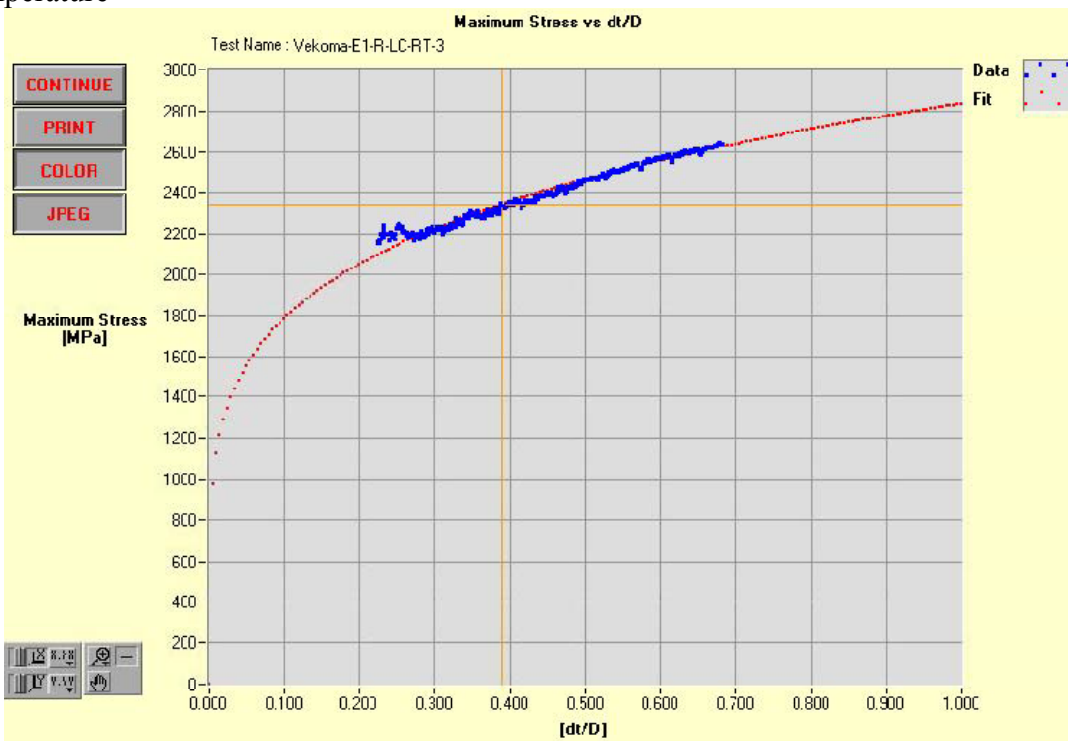


Figure 13. Specimen “E1” Satisfied the Critical Fracture Stress Model (2345 Mpa) at Room Temperature

Specimens “A” and “B” were analyzed according to the critical strain model and specimens “C,” “D”, and “E1” were analyzed according to the critical fracture stress model. Specimens “C,” “D”, and “E1” measured fracture toughness at -20C of $<95\text{MPa}\sqrt{\text{m}}$ or an equivalent Charpy impact energy of 26J which is lower than the 29J engineering requirement at ambient temperature.

Table 4.

Details of the Fracture Toughness Calculation from ABI Tests on the Five Specimens

Test Name	Yield Streng [MPa]	Est. Eng. UTS [MPa]	ABI BHN	Streng. Coeff., (K)	Strain Hard. Exp. [MPa]	Critical Stress [MPa]	Critical Depth (ht) [mic]	Critical Depth Ratio (dt/D)	WIDE [KJ/m ²]	KJc [MPa*m ^{0.5}]
Specimen A										
A-L-RT-1	317	488	168	731	0.134	2037	77.65	0.60	72.3	203
A-L-RT-2	322	481	167	712	0.128	2014	77.65	0.60	70.7	201
A-L-RT-3	318	486	169	726	0.132	2033	76.20	0.60	70.1	200
Average	319	485								201
Specimen B										
B-L-RT-1	319	488	168	729	0.133	2029	76.20	0.60	69.8	200
B-L-RT-2	325	501	172	749	0.134	2088	77.65	0.60	74.0	205
B-L-RT-3	329	491	171	726	0.128	2058	77.65	0.60	72.1	203
Average	324	493								203
Specimen C										
C-L-RT-1	375	586	199	884	0.137	2346	52.15	0.51	54.9	181
C-L-RT-2	383	590	202	884	0.135	2343	43.69	0.47	45.7	168
C-L-RT-3	380	604	204	916	0.141	2343	30.18	0.39	31.5	144
Average	379	593								164
Specimen D										
D-L-RT-1	374	590	199	893	0.139	2344	45.72	0.47	48.1	171
D-L-RT-2	382	581	199	866	0.132	2343	53.26	0.51	55.8	182
D-L-RT-3	373	582	198	876	0.137	2344	52.15	0.51	54.6	180
Average	376	584								178
Specimen E1										
E1-R-LC-RT-1	409	630	215	944	0.135	2345	22.02	0.34	23.1	128
E1-R-LC-RT-2	410	606	211	892	0.126	2345	37.03	0.43	38.1	156
E1-R-LC-RT-3	411	616	211	913	0.129	2343	30.18	0.39	30.6	143
Average	410	617								142

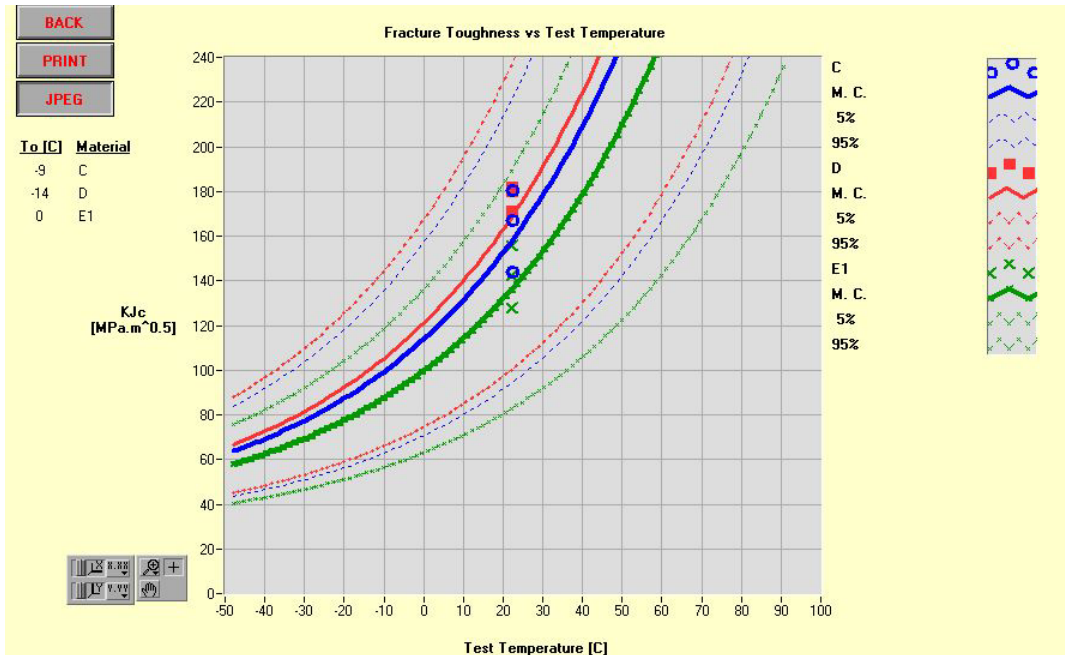


Figure 14. Shows the Fracture Toughness Master Curve (K_{Jc} Vs. Temperature) from Triplicate ABI Tests Conducted on Specimens “C”, “D”, And “E1”. The T_0 Values are -9°C , -14°C , and 0°C , Respectively

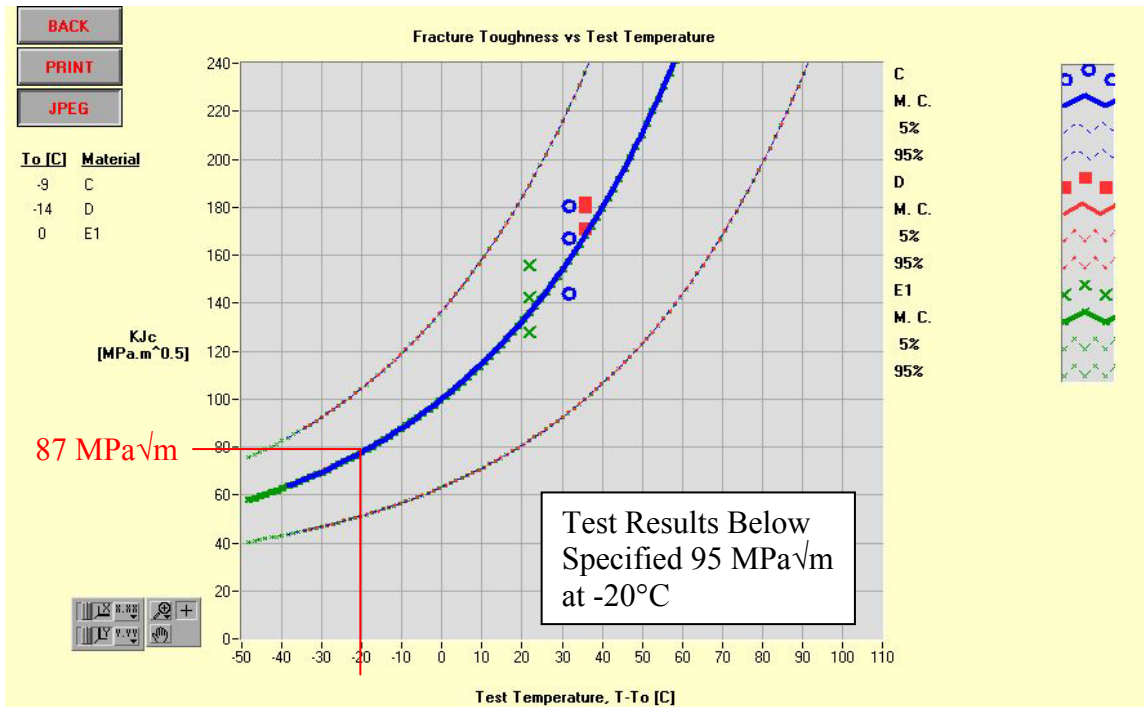


Figure 15. Shows a Normalized Plot of the Fracture Toughness Master Curve from Triplicate ABI Tests Conducted on Specimens “C”, “D”, and “E1”. The Reference Temperature T_0 is the Temperature at a Median Fracture Toughness Level of $100 \text{ MPa}\sqrt{\text{m}}$

Figures 14 and 15 show graphs of the master curves generated from specimens “C,” “D,” and “E1” both as tested in Figure 14 and normalized in Figure 15. Based on the 5% (dark blue) curve, at -20°C the equivalent fracture toughness value is 87 MPa√m, which is below the 95 MPa√m expected.

CHAPTER 3

RECOMMENDATIONS FOR IMPROVEMENT

Define Phase

How can the roller coaster manufacturer identify bad components from good components and replace the bad ones to circumvent an avoidable catastrophe? Can the proposed NDT method identify those components not properly heat treated? Can a business sustain the liability or bankruptcy due to the lawsuit for component or equipment failure?

Measure Phase

Based on Six Sigma principles the customer process performance requirements began with data gathering after critical to quality (CTQ) characteristics were established. The measurements used for collecting the necessary data and determining the outcome include; Round Robin results from an Interlaboratory Study (ILS) Program on the ABI Test, “Sampling Procedures and Tables for Inspection by Attributes in an acceptance sampling plan for lot Average Quality Level (AQL)” (ANSI/ASQ Z1.4, 2008).

Considerable effort was made to collect accurate data from the five laboratories that participated in the Inter-laboratory ABI Test study program by clear stating test instructions and procedures to be followed. The test data and calculations are summarized in the “Precision Summary for the ABI-Determined Yield Strength (YS-ABI)” table listed below in Table 5. This provided a way to quantify data acceptance sampling system for lot-by-lot inspection by attributes.

The reference to 1.4% average coefficients of variation (CV) CV% r sample data collected in Tables 6 and 7 “Precision Summary for the ABI-Determined Yield Strength

(YS-ABI)”, and “Precision Summary for the ABI-Determined Ultimate Tensile Strength (UTS-ABI)”, 1.5 % of AQL was designated as the baseline metric for sampling a lot size of 900 components. The Single Sampling Plan Normal Inspection II was selected for the sample code letter for 900 components under Table 10-1 Sample-Size Code Letters, Table I (ANSI/ASQ Z1.4, 2008). The sample code letter for this plan is “J.”

Precision and Bias Statements – Interlaboratory Study Program

The precision and bias statements are addressed in the Form and Style for ASTM Standards, in which precision is defined as; the closeness of agreement among test results obtained under prescribed conditions, and bias as; a systematic error that contributes to the difference between the mean of a large number of test results and an accepted reference value, March 21, 2010. In a recent article Kessel Nelson said, “The ILS Program helps insure that every ASTM International test method is validated by a precision statement outlining what users can expect from a specific protocol in terms of repeatability (i.e., what one laboratory analyzing the same sample multiple times would see as its range of acceptable results) and reproducibility (i.e., the differences that would be expected if the same sample were analyzed using the same method in multiple laboratories)” (Nelson, 2009).

ATC conducted an ILS Program for ABI testing where the results were very good. The president of ATC, Mr. Haggag, makes the following caveat about the study: “The precision of any of the various ABI-determined flow properties cited in these test methods is a function of the precision and bias of the various measurements of indenter diameter, the

precision and bias of the depth measurement, the precision and bias of the force measurement, and the precision and bias of the data acquisition system used to construct the force-depth curve. It is not possible to make meaningful statements concerning the precision and bias for all these measurements. However it is possible to derive useful information concerning the precision of the ABI-measured flow properties in a global sense from interlaboratory test programs. Values of the ABI-determined yield strength and true-stress versus true-plastic-strain curves were evaluated in (15) for several pressure vessel steels at various test temperatures. The ABI-derived yield strength and estimated ultimate strength values were evaluated in (16) for seven pipeline steels, with various grades and manufacturing dates, tested at room temperature using two indenter diameters (0.508 mm and 0.762 mm), and the ABI test results were compared to the results from tensile tests on the same materials” (Haggag, 2003).

An ILS Program provided the following results, in Table 5, for the CV for the most common ABI-measured flow properties:

Table 5.

Shows the CV% Data of the Most Common ABI-Measured Flow Properties from the ILS Program

	ABI-Yield Strength	ABI-Estimated Ultimate Strength	Strength Coefficient	Strain-Hardening Exponent	Uniform Ductility
*CV% _r	1.4	1.5	2.6	5.8	6.9
*CV% _R	1.7	2.3	3.4	6.7	7.8

*CV %_r = repeatability coefficient of variation in percent within a laboratory
 *CV %_R = repeatability coefficient of variation in percent between laboratories

In Table 6 an example is shown of the results for the most common ABI-measured flow properties from the participating laboratories and Table 7 is the precision summary

from just the yield strength measurements from the ILS Program (Form and Style for ASTM Standards, 2010).

Table 6.

A Precision Summary from the Yield Strength Measurements from the ILS Program

Materials	Average YS						
	(MPa)	Sr	CV% r	SR	CV% R	r	R
Al 6061-T651	329.97	5.41	1.64	6.28	1.90	15.15	17.58
Al 7075-T651	545.73	7.11	1.30	8.00	1.47	19.90	22.41
Steel 1018	361.90	6.10	1.69	7.21	1.99	17.07	20.18
Steel 4142	721.30	7.79	1.08	9.58	1.33	21.81	26.82
Average			1.40		1.70		

1) A simple sampling with an AQL of 1.5% to sample from a lot size of $N_2 = 900$ Components
 Select the plan from ANSI/ASQ Z1.4-2008

- Use sample size and acceptance number: 3
- General inspection level: II
- Sample size code letter: J (lot or batch = 501 - 1,200)
- Sample size $n_2 = 80$ (Table 10-2)
- Accept Number = 3
- Reject Number = 4

2) The α risk for this plan is = 3.40%

$$n_2 = 80 \quad \text{AQL} = 1.5\%$$

$$n_2 p = 80 \times 1.5\% = 1.2$$

$$P(A) = 1.2 \quad \text{Area} = 0.966 \quad (\text{Poisson Table})$$

$$\alpha = 1 - 0.966 = 0.034 \quad 3.40\%$$

3) The RQL for this plan (using a β risk of 10%) = 8.20%

$$n_2 = 80 \quad \text{AQL} = 1.5\%$$

$$\text{RQL} = 8.20\% \text{ (Table VI - A)}$$

4) The AOQL for this paln is = 2.40%

$$n_2 = 80 \quad \text{AQL} = 1.5\%$$

$$\text{AOQL} = 2.40\% \text{ (Table V - A)}$$

$$\text{A more accurate AOQL} = 2.19\% \text{ (Table V - A)}$$

Note: For a more accurate AOQL the values above must be multiplied by $[1 - (\text{sample size of } n_2 / \text{lot or batch size of } N_2)]$

From using 1.5% AQL a sample-size code letter “J” is selected (from Table 10-1) the sample size is 80, Ac (Acceptance number) is 3, and Rc (Non-acceptance or Reject number) is 4 (ANSI/ASQ Z1.4, 2008). The lot size of N_2 , the sample size of n_2 , and the acceptance number of c define a Single Sampling Plan. In this case, the lot size of N_2 components is 900, the sample size of n_2 is 80, and the acceptance number of c is 3; thus, a lot size with 900 components must have 80 components inspected. The lot will not be accepted if 4 or more nonconforming items are found in a sample size of 80 components. The results from the inspection method used reported that there were 60 components found to be nonconforming. In this case, the acceptance sampling system is not acceptable; therefore, a 100% inspection is necessary and is required.

Table 7.

Is the Sample-Size Code Letters (Table 1 of ANSI/ASQ Z1.4)

LOT OR BATCH SIZE	SPECIAL INSPECTION LEVELS				GENERAL INSPECTION LEVEL		
	S-1	S-2	S-3	S-4	I	II	III
2 - 8	A	A	A	A	A	A	B
9 - 15	A	A	A	A	A	B	C
16 - 25	A	A	B	B	B	C	D
26 - 50	A	B	B	C	C	D	E
51 - 90	B	B	C	C	C	E	F
91 - 150	B	B	C	D	D	F	G
151 - 280	B	C	D	E	E	G	H
281 - 500	B	C	D	E	F	H	J
501 - 1200	C	C	E	F	G	J	K
1201 - 3200	C	D	E	G	H	K	L
3,201 - 10,000	C	D	F	G	J	L	M
10,001 - 35,000	C	D	F	H	K	M	N
35,001 - 150,000	D	E	G	J	L	N	P
150,001 - 500,000	D	E	G	J	M	P	Q
500,001 and over	D	E	H	K	N	Q	R

Analyze Phase

Questions to consider for analysis include:

1. Can the roller coaster manufacturer produce quality coaster components for customers of the amusement parks?
2. Can the roller coaster components meet customer requirements?
3. How can the roller coaster manufacturer distinguish the good couplings from bad couplings?
4. Can the manufacturer improve components quality by producing conforming products to meet customer’s specifications and improve quality standard?

Table 8.

Some Important Factors to Consider that Contribute to Nonconforming Units When Determining Quality Analysis

Heat Treat	Outsource	Financial		Time Constraint	Components
Improperly heat treated.	Third party contractor	Profit		Construction time delays	Liabilities
Improperly quenched	Availability	Good parts	Bad parts	Time penalties	Safety
		Cost increase	Business retention		

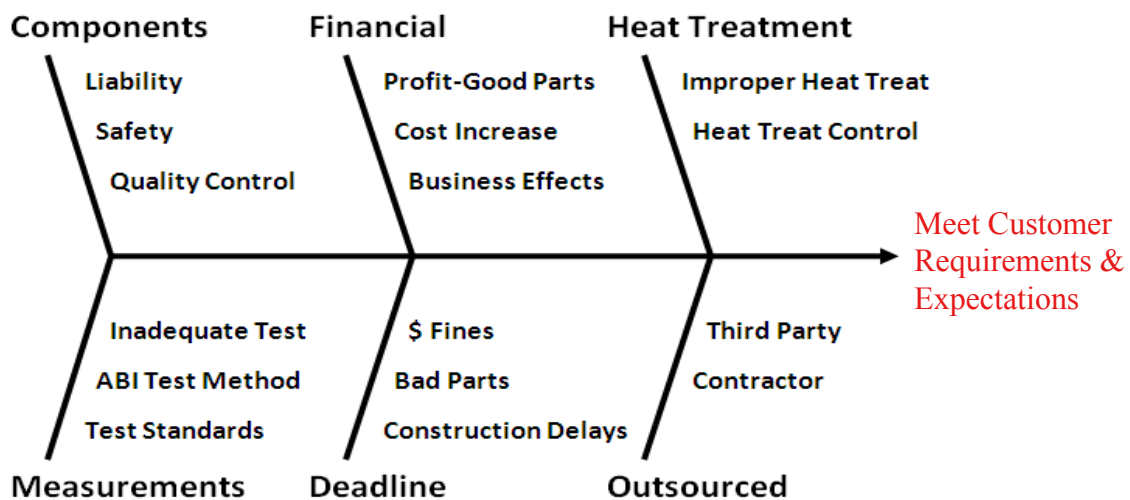


Figure 16. Shows the Cause-And-Effect “Fishbone” Diagram for Possible Contributors

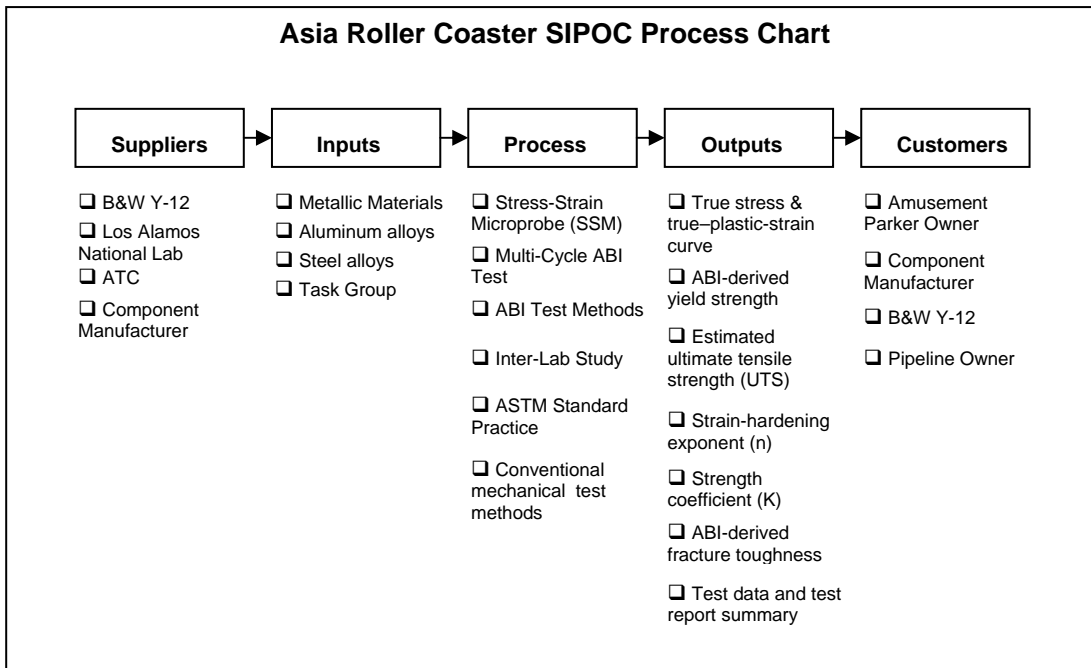


Figure 17. Shows the SIPOC Process Chart for Using SSM to Measure Mechanical Properties

Alpha (α) risk is described in terms of probability. The α risk for this plan is 3.4%. The Poisson distribution for Operating Characteristic (OC) Curve and AOQ (Average Outgoing Quality) Curve for this sampling plan are illustrated in Table 11. The calculations of α risk are as the following:

$$n_2 = 80; AQL = p = 1.5\%$$

$$n_2p = 80 \times 1.5\% = 1.2$$

$$P(A) = 0.966 \text{ (found from Table C Poisson Distribution } c = 3)$$

$$\alpha = 1 - 0.966 = 0.034 \text{ (3.4\%)}$$

The value $1 - \alpha$ (α) is the probability of accepting a lot with a percent nonconforming equal to the AOQ. The OC curve shows that a lot with a percent

nonconforming of 1.5% will be accepted, but there is with a risk of 0.034 (3.4%) of rejection. This is the α risk. The OC curve that shows 3.4 % of rejection for the producer for the lot of 900 components is illustrated in Figures 18 and 19.

The RQL (Reject Quality Level) or LQ (Limiting Quality) for this plan using a beta risk of 0.10 (10%) is 8.2% based on the $P(A) = P(c=3)$ on the OC curve. This means the consumer or customer risk if the process produces at 8.2% nonconforming, then 0.10 (10%) of the lots are accepted over time in the long run. The OC curve for the RQL that shows the probability of the lot with 8.2% will be accepted is illustrated in Figure 19. The ROL with 8.2% also can be found on Table VI-A Limiting Quality for Which $P_a = 10\%$ (for Normal Inspection, Single Sampling) (ANSI/ASQ Z1.4, 2008).

Table 9.

The Poisson Distribution for the Sampling Plan

The Poisson Distribution $P(c) = ((n_2 p_0)^c / c!) e^{-n_2 p_0}$ (Cumulative Values are in Parentheses)				
		$N_2 = 900$	Lot Size	
		$n_2 = 80$	Sample Size	
		$c = 3$	Acceptance Number	
<u>p</u>	<u>np</u>	<u>P(A)=P(c=3)</u>	<u>pP(A)</u>	<u>Calculation</u>
0.010	0.8	0.991	0.01	(=0.010 x 0.991)
0.015	1.2	0.996	0.015	(=0.015 x 0.996)
0.020	1.6	0.921	0.018	(=0.020 x 0.921)
0.025	2.0	0.857	0.021	(=0.025 x 0.857)
0.030	2.4	0.779	0.023	(=0.030 x 0.779)
0.040	3.2	0.603	0.024	(=0.040 x 0.603)
0.050	4.0	0.433	0.022	(=0.050 x 0.433)
0.060	4.8	0.294	0.018	(=0.060 x 0.294)
0.070	5.6	0.208	0.146	(=0.070 x 0.208)
0.080	6.4	0.116	0.009	(=0.080 x 0.116)

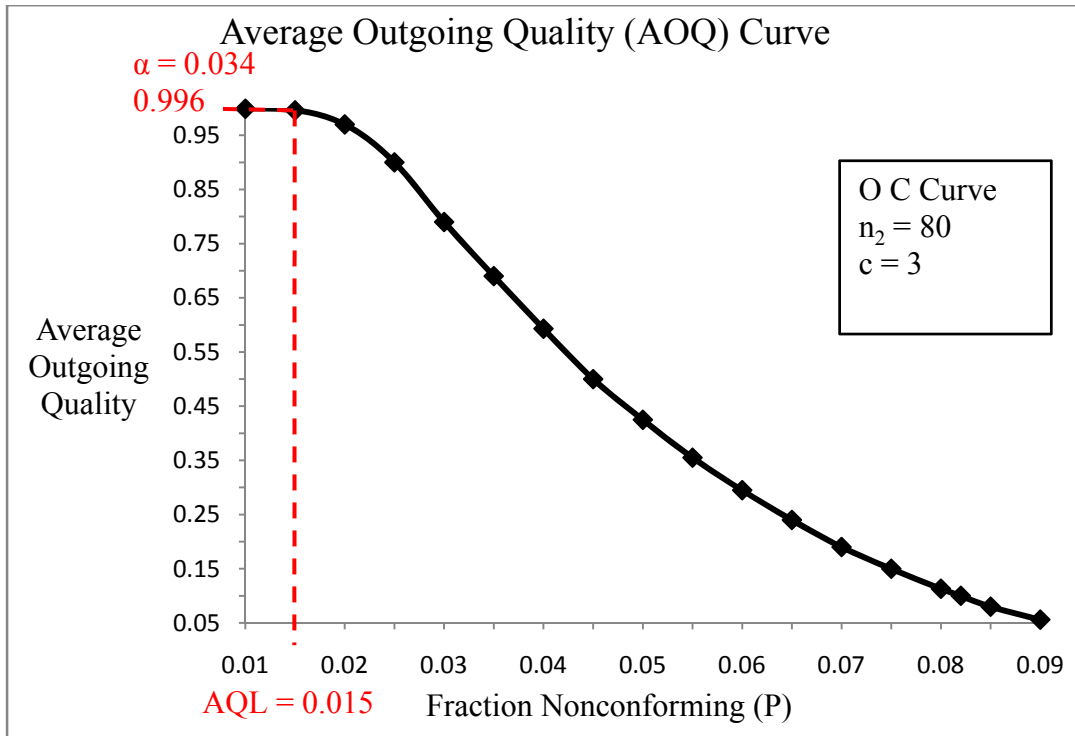


Figure 18. Shows the Manufacturers α Risk

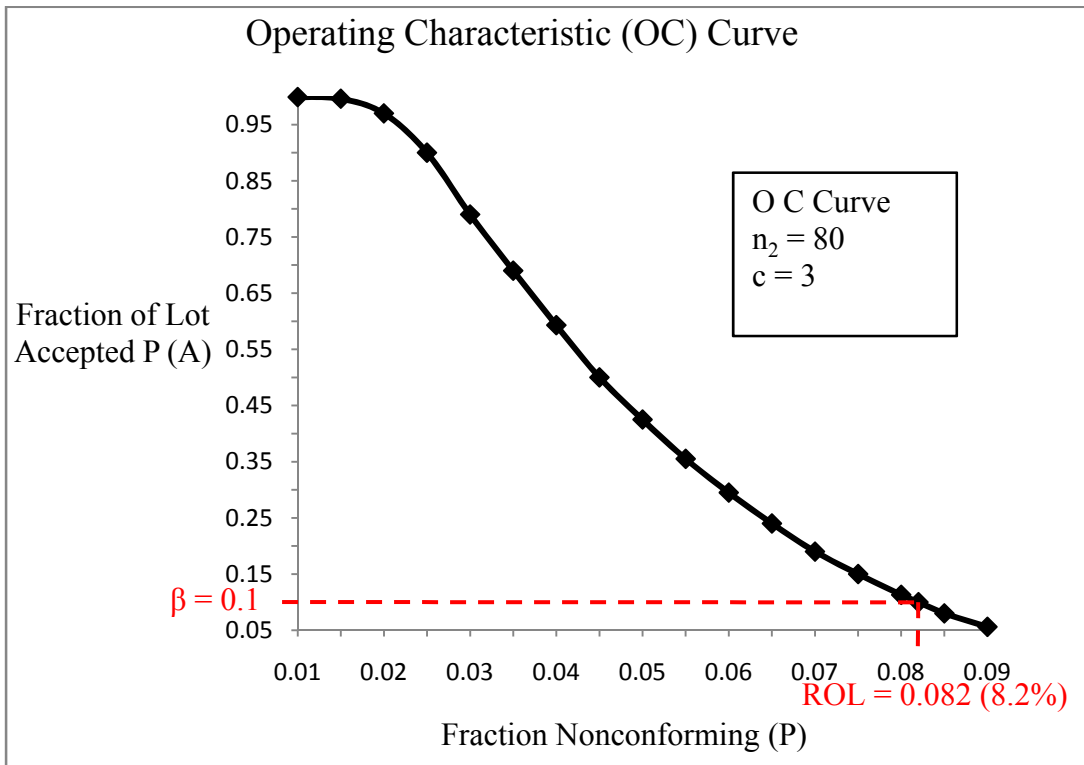


Figure 19. Shows the Consumer β Risk

The AOQ curve is illustrated in Figure 20. The AOQL (Average Outgoing Quality Limit) for this plan is 2.4% based on the pP (A) on the AOQ curve. From the AOQL curve with the peak at 2.4%, means the maximum average outgoing quality that will ever be seen while this plan in effect. The maximum average outgoing quality with 2.4% can also be found on Table V-A -- Factors for Determining Approximate Values for Average Outgoing Quality Limits for Normal Inspection (Single Sampling) (ANSI/ASQ Z1.4, 2008).

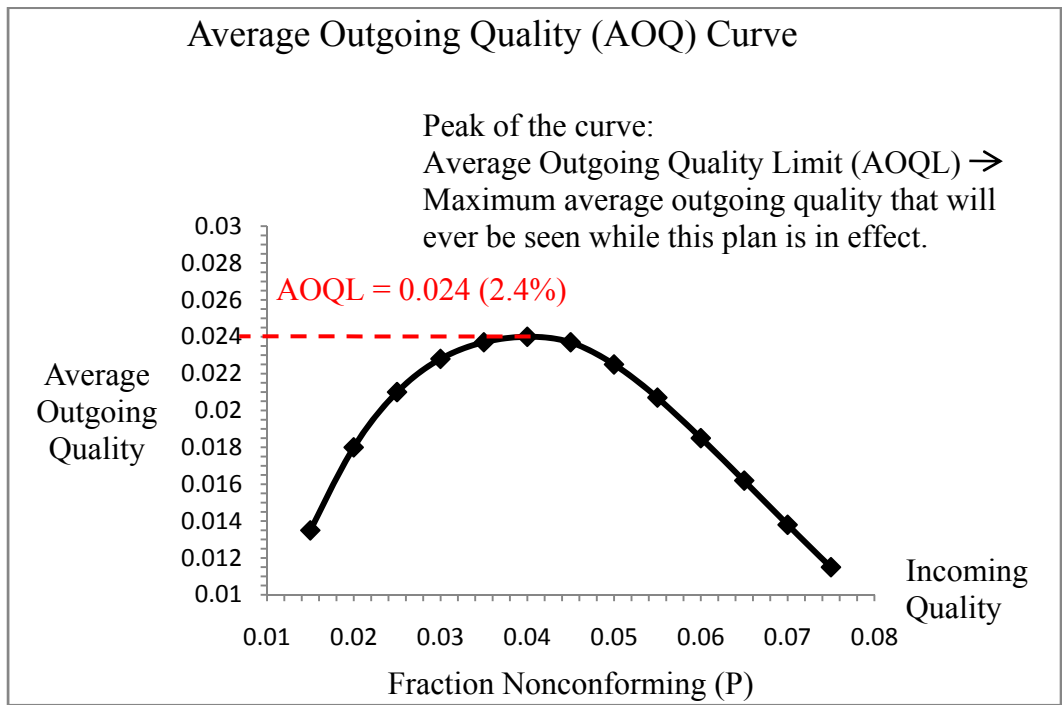


Figure 20. Shows the AOQ Curve That Includes the AOQL

Improvement Phase

The improvement phase should insure product quality by process enhancements to produce CTQ characteristic products to meet customer needs and wants. In order to improve quality components to meet customer’s specifications to reach ideal AQL, RQL, and AOQL, it is necessary that the roller coaster manufacturer take the first step to inspect the entire lot. Only the full inspection can identify conforming units from nonconforming

units and remove unacceptable components from the lot. Then, replace the nonconforming product with components that meet specifications.

The cost of inspecting 900 components is approximately \$860,000 based on the pricing from the ATC. The probability of roller coast equipment failure or ride accident is a realistic possibility according to the safer park database, which summarizes general product liability insurance for the roller coaster parts manufacturers of \$1,000,000 per claim or \$2,000,000 aggregate (General product liability, 2009). The cost of \$860,000 for 100% inspection of the entire lot of 900 components for the removal of defective components will reduce the probability of equipment or part failure in terms of monetary damage.

Control Phase

It is important to identify CTQ characteristics in the design stage of a new component. The CTQs are the critical quality parameters that relate to the wants and needs of the customer and what is important to the quality of the processes and services that ensure the final components meet the quality parameters and that contractual requirements will insure implicit quality. By identifying CTQ characteristics and ensuring that the design of a component addresses these characteristics, a project (like a new roller coaster) should meet expectation without rework or removal. Some type of tracking system established at the early stage of a component's design phase is the best way to monitor the process to ensure the components are manufactured within the control limits of the processes used. In the case of the roller coaster the fracture measurements were unknowingly outside the acceptable boundaries until after the components were in the final assembly stage at the construction site.

CHAPTER 4

CONCLUSIONS

No matter whether a roller coaster is being tested or a transmission pipeline, the need for unbiased NDT for fitness for service has never been more essential. Financial gain is probably the real motive for the construction company's decision to use test methods that are ineffective for this type of evaluation. Undoubtedly, the roller coaster was operating by the contractual deadline of January 2010 and with documentation that the construction and materials used meets the design expectations. However, in this instance the best NDT method was not selected, perhaps due to the cost of the testing, or perhaps due to conceptual bias against the ABI test. Regardless of the reason, the manufacturer is now in a difficult position of liability by accepting the uncertainty of the track couplings currently in use. The time lapse between when the track couplings were manufactured and made ready to be shipped to the construction site was sufficient for proper quality evaluation. This may have played a role in the decision by the construction company not to accept the penalties from a time overrun. The manufacturer knows that they are ultimately responsible for the product and that was apparent when they actively enlisted ATC's help in this matter. Hopefully the manufacturer is actively replacing all 450 couplings with 100% inspected components that will avoid any catastrophic failures and alleviate any liable responsibility in this regard, but we will never know.

This study is not an isolated case, but it seems to be a trend that needs closer examination. Even in the United States of America events like this occur, and sometimes the problem is ignored until the cost of not finding a solution becomes greater than reconciling the problem in the first place.

REFERENCES

- ANSI/ASQ Z1.4 (2008). Sampling procedures and tables for inspection by attributes. Retrieved from <http://webstore.ansi.org/RecordDetail.aspx?sku=ANSI%2FASQ+Z1.4-2008>
- ASTM Standards (2010). Form and style for ASTM standards, Retrieved from http://www.astm.org/COMMIT/Blue_Book.pdf
- Byun, T. S., Hong J. H., Haggag F. M. & Lee E. H. (1997). "Measurement of through-the-thickness variations of mechanical properties in SA508 Gr.3 pressure vessel steels using ball indentation test technique," *International Journal of Pressure Vessels and Piping*, Vol. 74, pp. 231-238.
- Davis, J. R. (1992). *ASM materials engineering Dictionary*, ASM International, December 1992.
- E1351-01(2006). Standard practice for production and evaluation of field metallographic Replicas, *ASTM International*, ASTM Standards on Disc, Section 3: Metals Test Methods and Analytical Procedures, Volume 03.01
- E1823-09a (2009). Standard terminology relating to fatigue and fracture testing, *ASTM International*, ASTM Standards on Disc, Section 3: Metals Test Methods and Analytical Procedures, Volume 03.01
- E1921-09a (2009). Standard test method for determination of reference temperature, T_o , for ferritic steels in the transition range, *ASTM International*, ASTM Standards on Disc, Section 3: Metals Test Methods and Analytical Procedures, Volume 03.01
- E975-03(2008). Standard practice for X-ray determination of retained austenite in steel with near random crystallographic orientation, *ASTM International*, ASTM Standards on Disc, Section 3: Metals Test Methods and Analytical Procedures, Volume 03.01
- General product liability (2009). Saferparks database, Retrieved from <http://www.saferparks.org/database/>
- Haggag, F. M. (1989). "Field indentation microprobe for structural integrity evaluation," U.S. Patent No. 4,852,397, August 1, 1989, Retrieved from <http://www.atc-ssm.com/papersreports.html>
- Haggag, F.M. (2002). In-service nondestructive measurements of stress-strain curves and fracture toughness of oil and gas pipelines: Examples of fitness-for-purpose applications. 5th international conference on pipeline rehabilitation & maintenance, Bahrain. Retrieved from <http://www.atc-ssm.com/papersreports.html>

Haggag, F. M. (2003). Round robin results of interlaboratory automated ball indentation (ABI) tests by task group e 28.06.14 (ABI test methods), ASTM International, April 11, 2003

Nelson, K. (2009). "Putting it to the test," *ASTM International Standardization News*, pp. 26-29, November/December 2009.

Rolfe, S. T. & Novak S. R. (1970). Slow bend K_{Ic} testing of medium strength high-toughness steels, ASTM, STP 463.

Tabor, D. (1951). The hardness of metals. *Oxford University Press USA*, Oxford Classics Series, reprinted 2000. ISBN13: 9780198507765 Available from <http://www.oup.com/us/>

APPENDIX: Article on the ABI Test (Haggag, 2002)

In-Service Nondestructive Measurements of Stress-Strain Curves and Fracture Toughness of Oil and Gas Pipelines: Examples of Fitness-for-Purpose Applications

Fahmy M. Haggag

Advanced Technology Corporation

1066 Commerce Park Drive

Oak Ridge, Tennessee 37830, USA

Tel: (865) 483-5756, E-Mail: Fahmy.Haggag@atc-ssm.com

Website: www.atc-ssm.com

ABSTRACT

The international transportation networks of oil and gas pipelines are becoming older and beginning to reach their design-lives. This situation brings concerns over pipeline rehabilitation as well as in meeting the current and future energy demands through increasing the transmission throughput safely. This paper describes applications of an innovative Stress-Strain Microprobe™ (SSM) system that utilizes an *in-situ* nondestructive Automated Ball Indentation (ABI) test technique to measure the stress-strain curves and fracture toughness of steel pipelines. The ABI tests provide the actual/current values of these key mechanical properties for base metal, welds, and heat-affected-zones. The SSM-measured key mechanical properties are used with other nondestructive measurements such as crack sizes (determined from smart-pig runs or from other on-line ultrasound devices) to determine the safe operating pressure of the pipeline or to necessitate certain actions of rehabilitation. Examples of SSM test results and their applications in fitness-for-purpose evaluations in the USA, Europe, and Asia, based on deterministic fracture mechanics analysis, are presented in this paper.

INTRODUCTION

Thousands of miles of gas and oil transmission pipelines currently in operation in the USA and other countries have no documentation of their mechanical properties. Section 49 of the US Code of Federal Regulations (CFR) part 192.107 (b) (2) stipulates that for the pipe which is not tensile tested, a yield strength of 165 MPa (24,000 psi) must be used in the equation that determines the design pressure of the pipe section. The Automated Ball Indentation (ABI) test is an *in-situ* nondestructive technique which measures several key mechanical properties of metallic materials. Furthermore, ABI tests provide the actual yield strength values of base metal, welds, and heat-affected-zones which, most of the time, are higher than the conservative CFR value of 165 MPa; thus natural gas or oil up-rating (increasing transmission throughput) can be accomplished safely. Hence, ABI testing of pipelines is a better alternative to the destructive and expensive mechanical tests as demonstrated by this work. This paper summarizes the flow (stress-strain) properties measured by the innovative ABI test technique on many pipeline materials. Moreover, when cracks and other pipeline flaws are produced due to service conditions (e.g. corrosion and/or mechanical damage), the ABI-measured fracture toughness values can be used in the deterministic structural integrity assessment of the pipeline based on fracture mechanics analysis. Examples of using ABI test results in fitness-for-service analysis are presented in this work.

The laboratory version of the patented [1] SSM system has been in commercial use since 1991 in three continents and the portable SSM version received a 1996 R&D 100 Award (considered by many researchers as the Nobel Prize of Applied Technology). Furthermore, in 1999 Advanced Technology Corporation (ATC) introduced a new miniature SSM system to provide even greater

portability and easier field applicability. Equipped with a small, portable battery pack and manual magnetic mounts, this system was proven to be a valuable test instrument for the pipeline industry. The accuracy, reliability, and easy field applicability of the SSM system to test pipeline materials with unknown properties have been demonstrated in this work on samples and on pipeline sections of several major natural gas operators.

The SSM system utilizes an Automated Ball Indentation (ABI) test technique that is described in detail in publications [1-11]. The ABI technique is nondestructive and localized, and is a sophisticated mechanical test technique which can be applied to small samples as well as to metallic components (such as natural gas and oil pipelines) in the field. These capabilities of the ABI technique and the SSM technology are advantageous and desirable for testing aged components and for structural integrity evaluation. One example of such applications is the problem caused by the lack of documentation on some natural gas and oil pipelines. Section 49 of the US Code of Federal Regulations (CFR) part 192.107 (b) (2) stipulates that for the pipe which is not tensile tested, a yield strength of 165 MPa (24,000 psi) must be used in the equation that determines the design pressure of the pipe section. Application of the SSM system to test these pipes will allow the determination of their safe operating pressure, and in many cases can allow up-rating (increasing the transmission pressure) for those pipelines when their SSM-measured yield strength is higher than the low/conservative value of 165 MPa (24 ksi). Furthermore, in addition to the ABI stress-strain curve measurements, the nondestructive and localized ABI technique of the SSM system can provide fracture toughness properties that cannot be obtained from the destructive (and costly for operating pipelines) tensile test. The determination of fracture properties from ABI tests are described elsewhere [7-9] but will be briefly summarized in this paper.

The ABI test is based on progressive indentation with intermediate partial unloadings until the desired maximum depth (maximum strain) is reached and then the indenter is fully unloaded. The indentation load-depth data are collected continuously during the test using a 16-bit data acquisition system. The nonlinear spherical geometry of the tungsten carbide indenter allows increasing strain as the indentation penetration depth is increased. Hence, the incremental values of load and plastic depth (associated with each partial unloading cycle) are converted to incremental values of true-stress and true-plastic-strain according to elasticity and plasticity theories [2,3]. The ABI test is fully automated (using a notebook computer, data acquisition system, and a servo motor) and a single test is completed in less than two minutes depending on the desired strain rate.

As part of this work, miniature tensile tests were fabricated from the pipeline materials with their axes in the circumferential direction. The ABI tests were conducted on the un-deformed end tabs of the miniature tensile specimens using the SSM system. Comparisons of the yield strength values and the stress-strain curves from the ABI and the miniature tensile tests show excellent agreement. Furthermore, a field demonstration of ABI testing was conducted on a 152-mm (6-inch) diameter section of a steel pipe using the new miniature SSM system where the testing head was temporarily mounted to the pipe using two manual magnets having on/off switches. The yield strength and the stress-strain curves from the ABI tests on the pipe are in excellent agreement with those from miniature and large tensile tests of specimens manufactured from the steel pipe. Another successful demonstration of the SSM system was made on a 610-mm (24-inch) diameter X52 steel pipe.

Field testing was also successful on a 914-mm (36-inch) diameter pipe in a refinery in Europe as well as on a 1168-mm (46-inch) diameter natural gas pipeline in Azerbaijan. This work demonstrates the major advantages of the SSM technology to the petroleum industry, namely, its nondestructive, localized, and *in-situ* capabilities. These features make the use of the SSM system, to nondestructively test pipelines with unknown properties, highly desirable to determine the safe operating pressure for the transmission and distribution of natural gas or oil without the need to cut

test coupons (e.g., hot tapping), machine destructive specimens, and repair the test areas. Since this work was completed, commercial use of the SSM system has produced hundreds of successful ABI tests on gas pipelines in the USA, Europe, and Asia.

RESULTS

Automated Ball Indentation (ABI) and miniature tensile tests were conducted at room temperature on seven materials obtained from two major natural gas operators, namely, ANR Pipeline Company and Columbia Gas Transmission Corporation. The ABI tests were conducted using 0.51-mm and 0.76-mm (0.020-inch and 0.030-inch) diameter tungsten carbide indenters on the end tabs of the miniature tensile specimens, fabricated with their axes in the circumferential direction. The ABI and miniature tensile tests were conducted using the laboratory bench-top configuration of the SSM system. Also as part of this work, the first field demonstration was conducted using the SSM-M1000 system outdoors where it was operated using a small booster battery pack and the testing head was temporarily attached to a 152-mm (6-inch) diameter pipe with two small manual magnets having on/off switches. A field configuration of the SSM system Model SSM-M1000 is shown in Fig. 1. An example of the indentation load-depth curve (using a 0.51-mm diameter indenter) and a typical comparison of the true-stress versus true-plastic-strain curves from ABI and tensile tests are shown in Fig. 2. Detailed summary tables and figures of ABI and tensile tests for all seven pipeline steel materials (Grade B, X42, X52, X60, X42, X52, and X65) are given in Reference [10] (available for downloading from ATC's website: www.atc-ssm.com).

The design of the miniature tensile test specimen was selected to allow manufacturing of specimens with their axes in the circumferential direction for all small and large diameters of the seven pipeline materials. This design was verified earlier at Oak Ridge National Laboratory (ORNL) where the yield strength and ultimate tensile strength values compared very well with those from large tensile specimens [11]. The ABI tests were conducted at room temperature on the end tabs of the miniature tensile specimens, and the stress-strain curves from both techniques were overlaid for comparison. All ABI tests were conducted using 0.51-mm and 0.76-mm (0.020-inch and 0.030-inch) diameter tungsten carbide indenters at indentation speed of 0.0076 mm/s (0.0003 inch/s). The two indenters produced excellent results. However, the smaller size of 0.51-mm (0.020-inch) diameter is more advantageous for use in the field with small, manual magnetic mounts since the maximum indentation load will be less than 400N (90 pounds).

The true-stress and true-plastic-strain values were calculated from the ABI load-depth data using Equations Number 2 through 9 (Ref. 2) where the constraint value " α_m " was taken as 1.3 and 1.2 for the 0.51-mm and 0.76-mm (0.020-inch and 0.030-inch) diameter indenters, respectively. The yield strength value was calculated according to Equations 10, 11, and 14 of Reference [2]. The values of the yield-strength offset-constant and the yield strength slope (Equation 14 in Ref. 2) were determined as -238.6 MPa and 0.3585 (-34.6 ksi and 0.3585) for the 0.51-mm (0.020-inch) diameter indenter while these values were -284.8 MPa and 0.4273 (-41.3 ksi and 0.4273) for the 0.76-mm (0.030-inch) diameter indenter. The true-stress and true-plastic-strain results (including the yield strength point) were fitted to the power law form of Equation 1 of Ref. [2] in order to determine the strain-hardening exponent (equivalent to uniform ductility) and the strength coefficient.

Comparison of the yield strength from ABI tests, using the 0.51-mm and 0.76-mm (0.020-inch and 0.030-inch) diameter indenters, with those from the miniature tensile specimens is shown in Fig. 3. As shown in this figure, the yield strength from ABI tests (using both indenter sizes) and from tensile tests are in excellent agreement where most of the data fell between the $\pm 5\%$ dashed lines bounding the perfect agreement line (45-degree solid line). A similar agreement was obtained for the

ultimate strength values from ABI tests with those from the miniature tensile specimens. Hence, Figs. 2 and 3 demonstrate the reliability and the accuracy of the ABI test technique for testing pipelines.

Demonstration of SSM Field Testing of Pipelines

The initial ABI testing of a 152-mm (6-inch) diameter carbon steel pipe with a nominal thickness of 7-mm (0.27 inch) was conducted using three sizes of tungsten carbide indenters: 1.57-mm, 0.76-m, and 0.51-mm (0.062-inch, 0.030-inch, and 0.020-inch) diameter. The testing head of the SSM system was mounted on the pipe using four aluminum V-blocks [10]. Test results on smoothly machined areas were in very good agreement with those from locally polished areas. All ABI tests were carried out up to a maximum indentation depth of 30% of the indenter radius. The true-stress/true-plastic-strain curves from all three indenter sizes produced the same stress-strain curves despite the various test volumes sampled for each ABI test.

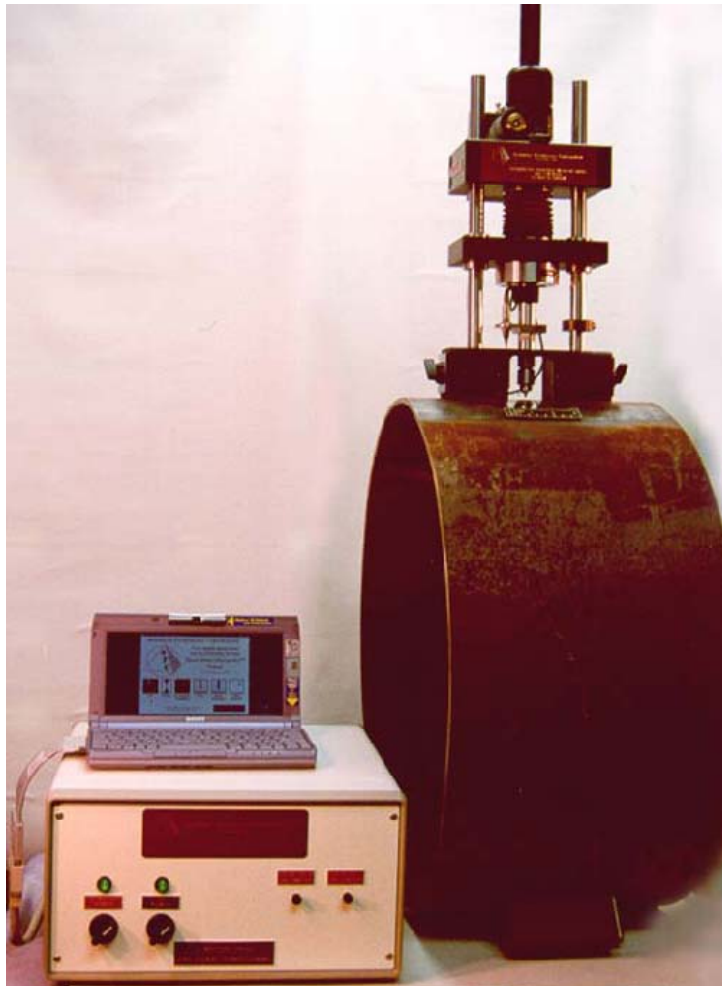
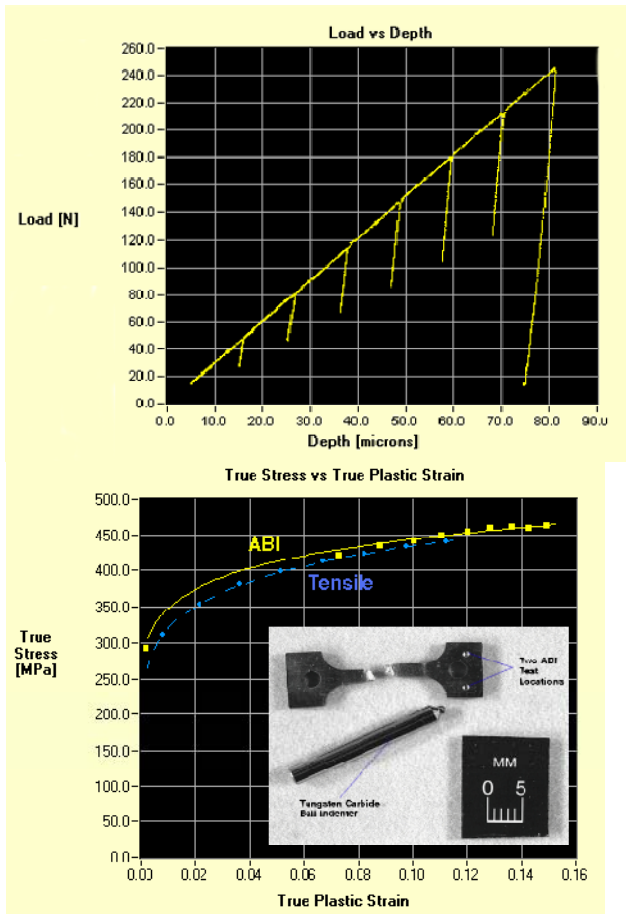


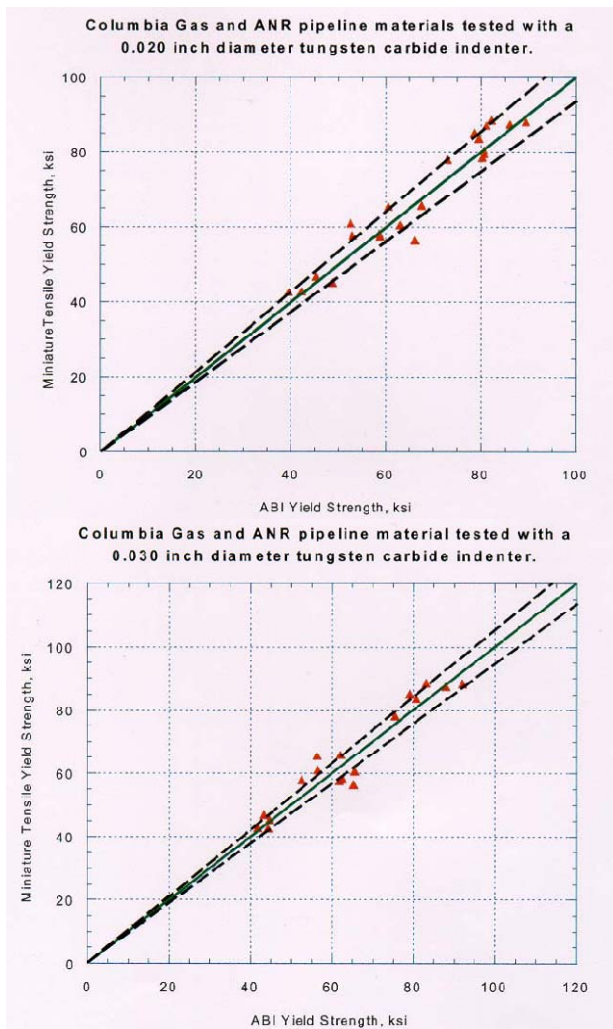
Fig. 1 The Testing Head of the Miniature SSM System is Mounted (Using Manual Magnets) on a 610-mm (24-Inch) Diameter X52 Steel Pipe Section.



(a)

(b)

Fig. 2 (a) Indentation Load Versus Depth in an ABI Test Using a 0.51-Mm (0.02-Inch) Diameter Tungsten Carbide Indenter on X42 Ferritic Steel Material. (b) True-Stress Versus True-Plastic-Strain Curves from ABI and Tensile Tests on X42 Pipeline Steel. A Miniature Tensile Specimen is Shown With Two Indentations Made on One End Tab With The 1.57-mm Diameter Tungsten Carbide Indenter Shown in the Inset Photo.



(a)

(b)

Fig. 3 Comparison Between Yield Strength From ABI Tests and Miniature Tensile Tests: (A) Using a 0.51-mm Diameter Indenter, (B) Using a 0.76-mm Diameter Indenter. The Dashed Lines Represent the $\pm 5\%$ Variation From Perfect Agreement (45-Degree Solid Line). (1 ksi = 6.895 MPa).

A field demonstration was conducted using the miniature Portable/In-Situ Stress-Strain Microprobe system (Model SSM-M1000) outdoors where it was operated using a small booster battery pack and the testing head (weighing 10 kg) was temporarily attached to a 152-mm diameter carbon steel pipe (obtained from Columbia Gas Transmission Corporation) with two small manual magnets having on/off switches. Both the 0.51-mm and 0.76-mm (0.020-inch and 0.030-inch) diameter indenters produced successful ABI test results using the magnetic mounts. The yield strength and stress strain curves from ABI tests on the pipe section and on the end tabs of miniature tensile specimens (fabricated from the pipe section) were in very good agreement with those from the test results of miniature tensile specimens. Another successful SSM field demonstration was conducted on a 610-mm (24-inch) diameter X52 pipeline.

Determination of Fracture Toughness Master Curve from ABI Tests

Indentation with a small ball indenter generates concentrated stress (and strain) fields near and ahead of the contact of the indenter and the test surface, similar to concentrated stress fields ahead of a crack albeit the indentation stress fields are mostly compressive. The high value of the stress under the ball indenter is sometimes called an example of *plastic constraint* where it is the rigid material surrounding the indentation volume that does the constraining. Hence, at a certain critical ball indentation depth there is a high state of transverse and lateral stresses similar to those in front of a sharp notch in an elastic material. Although, the conditions for crack initiation might be attained, the high degree of plastic constraint is the reason that cracks do not develop during ball indentation of ductile metallic materials. This explains that only initiation fracture toughness and no tearing modulus can be determined from ball indentation. The initiation fracture toughness is calculated from the integration of indentation deformation energy up to the critical depth (when the maximum pressure underneath the ball indenter equals the critical fracture stress of the steel material) as described in detail elsewhere [7, 9]. Examples of the ABI-measured fracture toughness results on plate and weld steel materials are shown in Figs. 4 and 5. The new ABI-measured fracture toughness capability is, in practical terms, material thickness independent (since small indenters can be used for all pipelines and pressure vessels). Furthermore, its localized nature allows testing heat-affected-zones that cannot be tested destructively because of their irregular shape and small volumes.

How can fracture toughness of ferritic steels be determined from the ABI test?

It is agreed upon that an ABI test does not produce fracture in a metallic test sample (because of the plastic constraint and the ductility of the test material) and that there is no fatigue crack requirement for the ABI test (which makes it nondestructively attractive). However, the simple reasons (without the use of equations) for

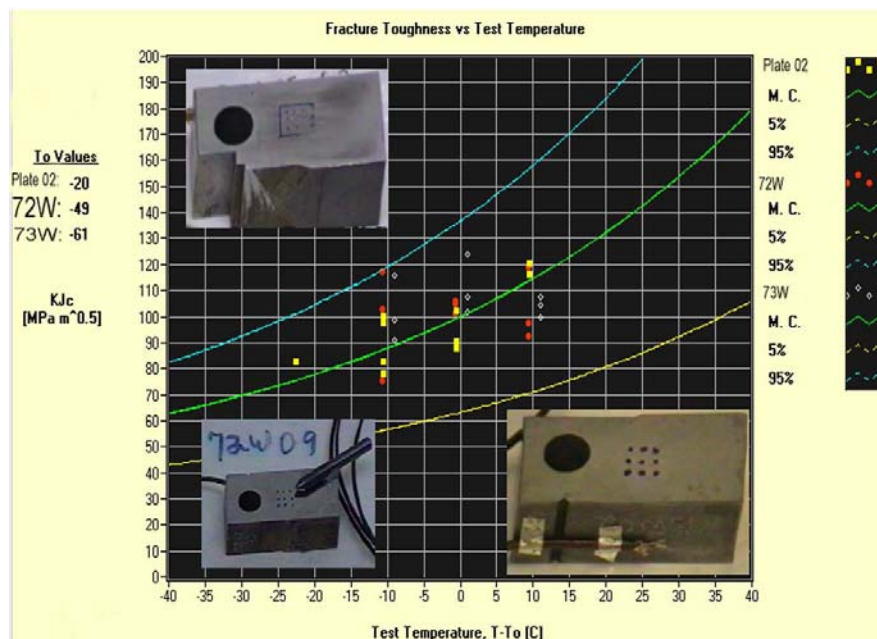


Fig. 4 Fracture Toughness Master Curve Obtained from ABI Tests on Three Reactor Pressure Vessel Steels. A 0.51-mm (0.020-Inch) Diameter Tungsten Carbide Indenter was Used to Perform 11 ABI Tests on Plate 02 (The Specimen on the Top Left of the Figure), and 9 ABI Tests Each on the 72W and 73W Weld Samples (Shown on the Left and Right Lower Part of the Figure, Respectively). The

ABI-Determined Reference Temperatures of the Three Materials were Within 5°C of the Values from the Pedigreed Destructive Fracture Toughness Tests.

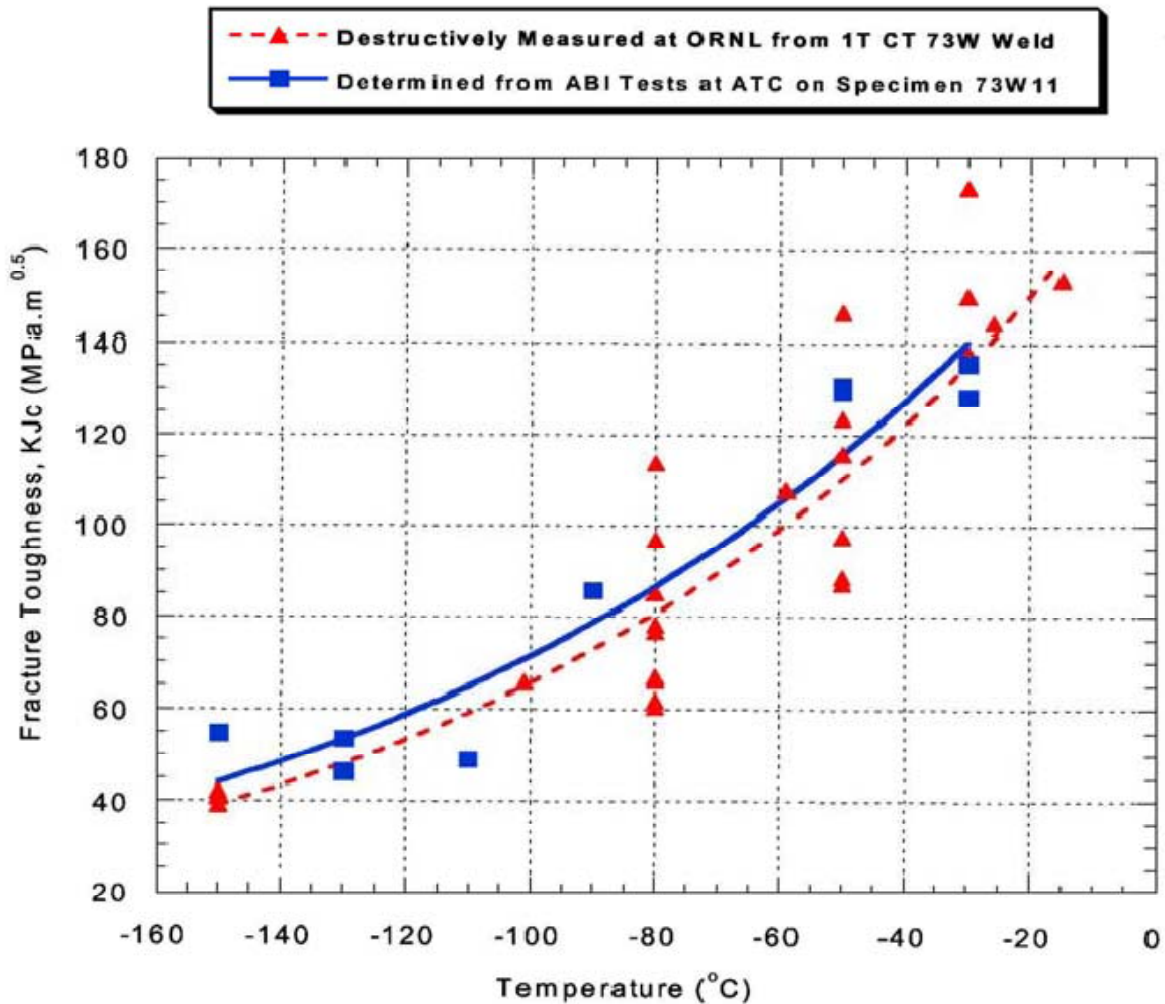


Fig. 5 Comparison Between Nondestructively ABI-measured (K_{Jc}^{ABI}) Performed at ATC (using a 1.57-mm Indenter) and Destructive 1T CT Fracture Toughness Test Results of 73W Weld of ORNL.

the success of this technique to determine fracture toughness of ferritic steels in the transition region are: (1) the attainment of a high degree of stress-triaxiality (stress concentration similar to that ahead of a crack-tip) because of the plastic constraint provided by the test material surrounding the spherical indentation, (2) the increase of the value of maximum stress (110% of the mean pressure in the material beneath the ball indenter) with increasing indentation depth until reaching or exceeding (at some low test temperatures) the critical fracture stress of the material, and (3) the fracture of ferritic steels at low temperatures in the transition region is controlled by the critical fracture stress of the material.

At a critical indentation depth (when the maximum stress underneath the ball indenter equals the critical fracture stress), the deformation energy (integration of the area under the indentation load versus indentation depth up to the critical indentation depth, in the same units as the J-integral) represents the temperature dependent part of the fracture toughness of the test material. A

temperature-independent value of $30 \text{ MPa}\sqrt{\text{m}}$ is added to the ABI-determined fracture toughness value, similar to the equation of the fracture toughness master curve of ASTM Standard E1921-97. The fact that during an ABI test all the requirements to calculate the initiation fracture toughness are achieved at a critical deformation energy depth allows the determination of fracture toughness without any crack propagation (the latter is prevented by the high plastic constraint of the test material surrounding the spherical indentation). Hence, only fracture toughness initiation and no tearing modulus can be determined from the ABI test.

Researchers at ATC have produced cracks in two perpendicular directions in a sodium chloride single crystal using a 1.5-mm diameter ball indenter (work performed by ATC for the US Navy, see Fig. 6) which is a proof that the maximum stress underneath the ball indenter reached the fracture stress of the single crystal.

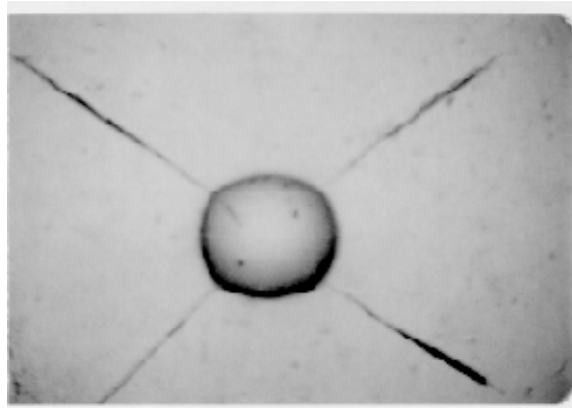


Fig. 6 Cracks Produced with a 1.5-mm Diameter Ball Indenter in a Sodium Chloride Single Crystal.

Moreover, in the non-standardized bulge test (sometimes called small punch test) a very thin sheet of metal is clamped in a die, and a punch with a large spherical end is pushed against one surface of the thin sheet until the sheet is fractured on the opposite/tensile side. However, fracture toughness cannot be calculated from the plane stress bulge test. In the bulge test, fracture occurs even though the specimen does not contain any fatigue crack prior to the test.

In an ABI test, the maximum stress underneath the indenter increases with depth but fracture does not occur because of the plastic constraint of the material surrounding indentation (the specimen or the structure thickness must be ten times the maximum indentation depth to avoid back surface effects and to obtain valid ABI test results). Furthermore, in a destructive J_{IC} fracture toughness test, although we propagate/extend the fatigue crack, we extrapolate the power-law-fit of the J-integral versus crack extension curve to intersect a line parallel to the blunting line (0.2 mm offset line) where the intersection point determines the J_{IC} initiation fracture toughness. This procedure is required since it is very difficult to stop loading the sample at the appropriate deformation energy level associated with the onset of crack extension from the pre-existing fatigue crack of the destructive fracture toughness specimen. This means that the fracture toughness value determined from the destructive test is actually the deformation energy up to the point of initial crack extension. Hence, the capability to determine fracture toughness from the ABI test without having to machine and fatigue crack a specimen is a truly innovative method, and it is the only method for *in-situ* direct measurement.

Furthermore, the current and challenging need for numerous industrial applications is to obtain fracture toughness of ferritic steel structures without cutting boat samples or hot tapping to machine miniature fracture specimens. Miniature specimens produce invalid fracture toughness values most of the time because of the violation of the geometry requirements for plane strain. For example,

many pipelines and vessels are not manufactured in the large thickness required to obtain valid fracture toughness test results, and often the owner of such components will not allow hot tapping or the cutting of a boat sample regardless of its size. Moreover, ABI tests will produce valid fracture toughness values all the time while the current ASTM destructive methods may never produce valid test results. Another great advantage of the ABI test method is its applicability to small welds and heat-affected-zones where the current ASTM standard test techniques might not be feasible.

Moreover, recent developments at ATC allow ABI testing at ambient temperature and determining the fracture toughness at other temperatures of interest (using the fracture toughness master curve concept and the appropriate critical fracture stress or strain model depending on the actual test temperature). Furthermore, dynamic fracture toughness values could be estimated from the measured static fracture toughness and yield strength test results.

Determination of the Indentation Energy to Fracture (*IEF*)

A new ABI energy parameter called *Indentation Energy to Fracture (IEF)* was developed for ferritic steels [7]. This *IEF* parameter allows the nondestructive determination of fracture energy from the ABI-measured mean indentation pressure up to a critical indentation depth (according to the controlling micro-mechanical fracture mechanism of the critical fracture stress or the critical fracture strain, depending on the test temperature). The indentation load versus depth curves from ABI tests at various temperatures were used together with the critical fracture stress model to determine the fracture toughness from the indentation deformation energy. The development of the *IEF* parameter is based on the following:

- (a) Fracture toughness can be interpreted as the deformation capability of the material under a concentrated stress field.
- (b) Indentation with a small ball indenter generates concentrated stress (and strain) fields near and ahead of the contact of the indenter and the test surface, similar to concentrated stress fields ahead of a crack albeit the indentation stress fields are mostly compressive. The high value of the stress under the ball indenter is sometimes called an example of ***plastic constraint*** where the rigid material surrounding the indentation volume that does the constraining. Hence, at a certain critical ball indentation depth there is a high state of transverse and lateral stresses similar to those in front of a sharp notch in an elastic material. Although, the conditions for crack initiation might be attained, the high degree of plastic constraint is the reason that cracks do not develop during ball indentation of ductile metallic materials. This explains that only initiation fracture toughness and no tearing modulus can be determined from ball indentation.
- (c) Monotonic tensile and compressive stress-strain curves are similar which is true for most homogenous metallic structural materials.
- (d) The cleavage fracture stress in ferritic steels is nearly temperature insensitive at very low test- temperatures in the transition and low shelf regions.
- (e) The deformation energy due to ball indentation up to a limit mean pressure level is related to the fracture toughness; the limit stress, attained at a critical indentation depth in an ABI test, is proportional to the critical fracture stress of the test material.

The *IEF* is thus defined as:

$$IEF = \int_0^{h_f} P_m(h) dh \quad (1)$$

where,

$$P_m = 4P / \pi d^2 \quad (2)$$

In the above equation, P_m is the mean indentation contact pressure, P is the indentation load, h is the indentation depth, h_f is the indentation depth when the value of the mean pressure multiplied by 1.1 is equal to the critical fracture stress (i.e. $P_m \times 1.1 = \text{fracture stress}$), and d is the chordal diameter of the indentation. It is important to note that the mean pressure under a spherical indentation increases with increasing indentation depth and with decreasing test temperature in ferritic steels.

$$d = 2(Dh - h^2)^{0.5} \quad (3)$$

Determination of fracture toughness $(K_{JC})^{ABI}$ from ABI tests at various temperatures

The Charpy impact energy and the static fracture toughness, K_{JC} , have non-zero lower shelves even at very low test temperatures. Hence, the fracture energy per unit area, W_f can be given by:

$$W_f = W_0 + W_T \quad (4)$$

where W_0 is the lower shelf energy per unit area, and W_T is the temperature-dependent energy to be calculated from Equation 1 (i.e. , $W_T = IEF$).

For ferritic steels (with yield strength of 275 to 825 MPa or 40-120 ksi) the fracture toughness (median value) versus temperature curve in the transition temperature region is expressed by the master curve (ASTM E-1921-97):

$$K_{JC} (med) = 30 + 70e^{0.019(T-T_0)} \text{ MPa}\sqrt{\text{m}} \quad (5)$$

where T is the test temperature and T_0 is the reference temperature when $K_{JC} = 100 \text{ MPa}\sqrt{\text{m}}$. From the above equation, the lower shelf fracture toughness, W_0 , is $30 \text{ MPa}\sqrt{\text{m}}$. The fracture toughness determined from ABI tests can then be calculated from:

$$(K_{JC})^{ABI} = 30 + \sqrt{2E(W_T)} \quad (6)$$

where E is the elastic modulus.

Example of the Use of ABI tests in a Fitness-for-Service Assessment

A catastrophic failure occurred in a natural gas plant in a cold winter night shortly following the leak of a liquid natural gas into the line. The combination of cold temperature and high strain rate near a crack resulted in the destruction of approximately 12-meter section of a 508-mm (20-inch) diameter pipeline into several hundred small pieces. The plant operator was concerned that the pipeline steel might not have the appropriate flow and fracture properties since the fracture surfaces of many small pieces indicated brittle fracture. Although, the pipeline piece containing the crack was not found at the time of ATC's report, the ABI tests on several small pieces confirmed that the pipeline steel material meet the mechanical properties specified for the seamless carbon steel pipe at the time of construction. Multiple ABI tests were conducted, on a block machined from a small steel piece, at several low temperatures using ATC's patented Portable/In-Situ SSM system. All ABI tests were

conducted using a 0.51-mm (0.020-inch) diameter tungsten carbide indenter at a speed of 0.01-mm/s (0.0004 in/s), or a strain rate of 0.014/s, to a maximum indentation depth of 0.076-mm (0.003-inch). Stress-strain curves and fracture toughness values were measured from the individual ABI tests. In addition, the fracture toughness median curves, as well as its 95% and 5% confidence limit curves, were determined from the ABI tests. The reference temperature, T_0 , defined in the ASTM Standard E1921-97 [Ref. 12, “Standard Test Method for Determination of Reference Temperature, T_0 , for Ferritic Steels in the Transition Range,”] as the test temperature corresponding to a median fracture toughness level of 100 MPa \sqrt{m} (90.9 ksi \sqrt{in}), was determined from the ABI tests at several low test temperatures. The ABI tests determined a T_0 value of -24°C for the base metal of the pipe. The ABI-determined T_0 value demonstrates that the pipeline material has good static fracture toughness of 100 MPa \sqrt{m} at a low temperature of -24°C that is lower than normal pipeline operating temperature in winter. However, these ABI-measured good static fracture toughness values do not prevent brittle failure that might result from the existence of any small crack (developed during pipeline service) and due to the combination of very low temperature and a dynamic loading at a high strain rate (it should be noted that all carbon steels have a lower/brittle fracture toughness shelf with a median value of 30 MPa \sqrt{m} regardless of their various values of much higher fracture toughness at higher operating temperatures).

The fracture toughness values were calculated from ABI tests according to the procedures described in Reference 7. Examples of the graphical and printed test data and results from a single ABI test [ML-28-4 conducted at -33°C (-28°F)] are shown in Figures 7-11. Fig. 7 shows the ABI indentation load versus depth data using a single-cycle ABI test technique (without any intermediate partial unloading). The yield strength calculation plot is shown in Fig. 8 where “P” is the load, “dt” is the chordal diameter of indentation at various depth values, and “D” is the indenter diameter. Figure 9 shows the true-stress/true-plastic-strain curve where the yield strength value (plotted as a solid symbol) was calculated from Fig. 8 as described in Reference 2. Fig. 10 shows the maximum pressure (calculated as 110% of the mean pressure underneath the indenter as discussed in Reference 7) as a function of normalized indentation depth (dt/D). It is important to note that the maximum pressure increases with increasing indentation depth. When the value of the maximum stress equals the critical fracture stress (340 ksi) the critical “dt/D” is used to calculate the critical indentation depth for integrating the area under the indentation load/depth curve to calculate the J-integral and the fracture toughness of the test sample. In this ABI example, the critical “dt/D” and the critical indentation depth are 0.31 and 12.45 microns as shown on the printed test results shown in Fig. 11. The ABI-determined fracture toughness reference temperature (T_0) value is -24°C. The fracture toughness median curve and its 95% and 5% confidence limit curves are shown in Figure 12.

In Figure 10, note that the maximum stress at this low test-temperature of -33°C (-28°F) increases well beyond the critical fracture stress up to a value of 2760 MPa (400 ksi) at a dt/D value of 0.75 (the later represents the end of the ABI test at a depth of 12.45 microns). The high values of the maximum stress were attainable because of the multi-axial nature of the ABI test that provides a high degree of stress-triaxiality (stress concentration) underneath the spherical indenter due to the high degree of plastic constraint provided by the ductile material surrounding the indentation. This is in contrast to the uniaxial tensile test that does not provide enough constraint in the specimen gage section, and its maximum stress is attained at the ultimate tensile strength (specimen necking). The ultimate strength for many structural steels is less than 830 MPa (120 ksi) that is much lower than the critical fracture stress of the material. Figure 9 illustrates that although the ABI test provides tensile properties, it also measures fracture toughness because of its triaxial stress loading nature. Several text books describe the area under a tensile stress-strain curve as an estimate of fracture toughness which is incorrect since the tensile test does not provide the required constraint and its units are in MPa (ksi) and not in the appropriate fracture toughness units of MPa \sqrt{m} (ksi \sqrt{in}).

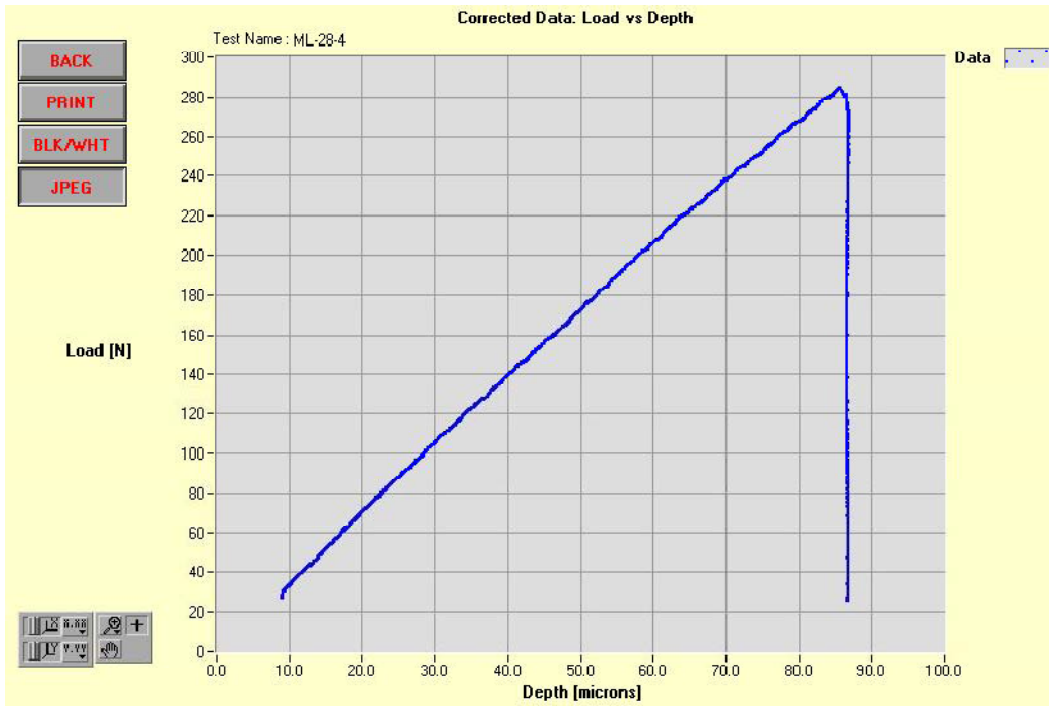


Fig. 7 Indentation Load versus Depth using the Single-Cycle ABI Test Technique.

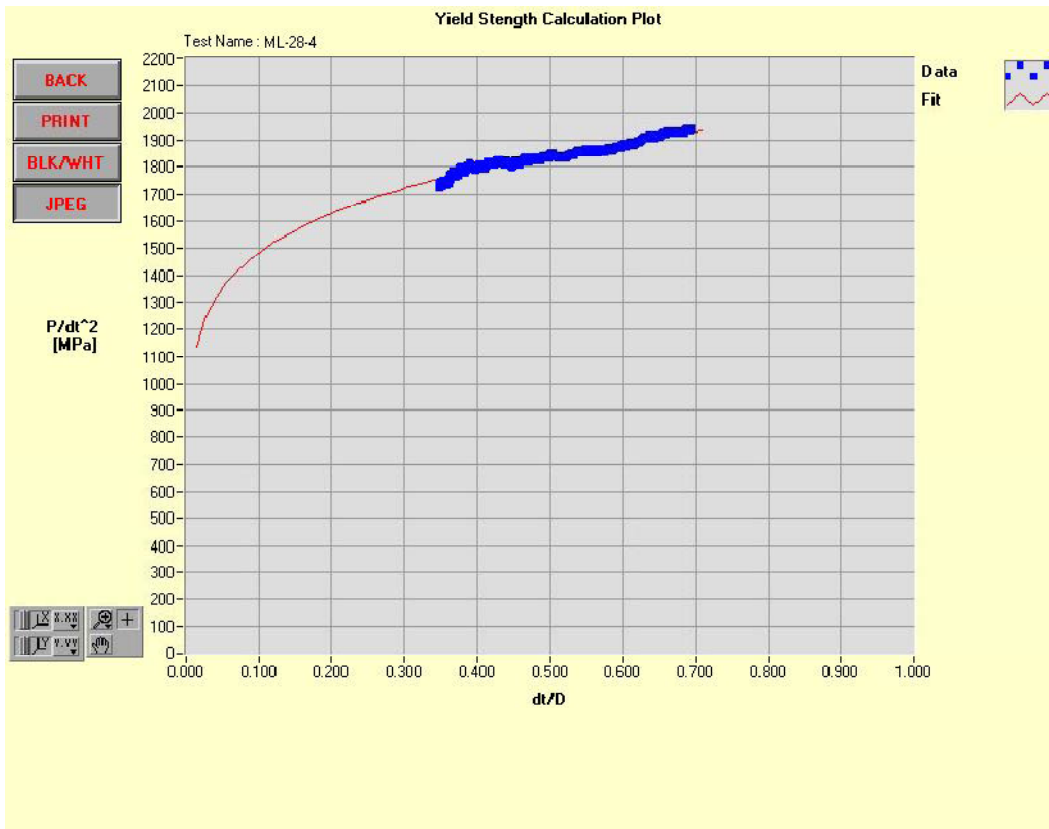


Fig. 8 Yield Strength Calculation Plot.

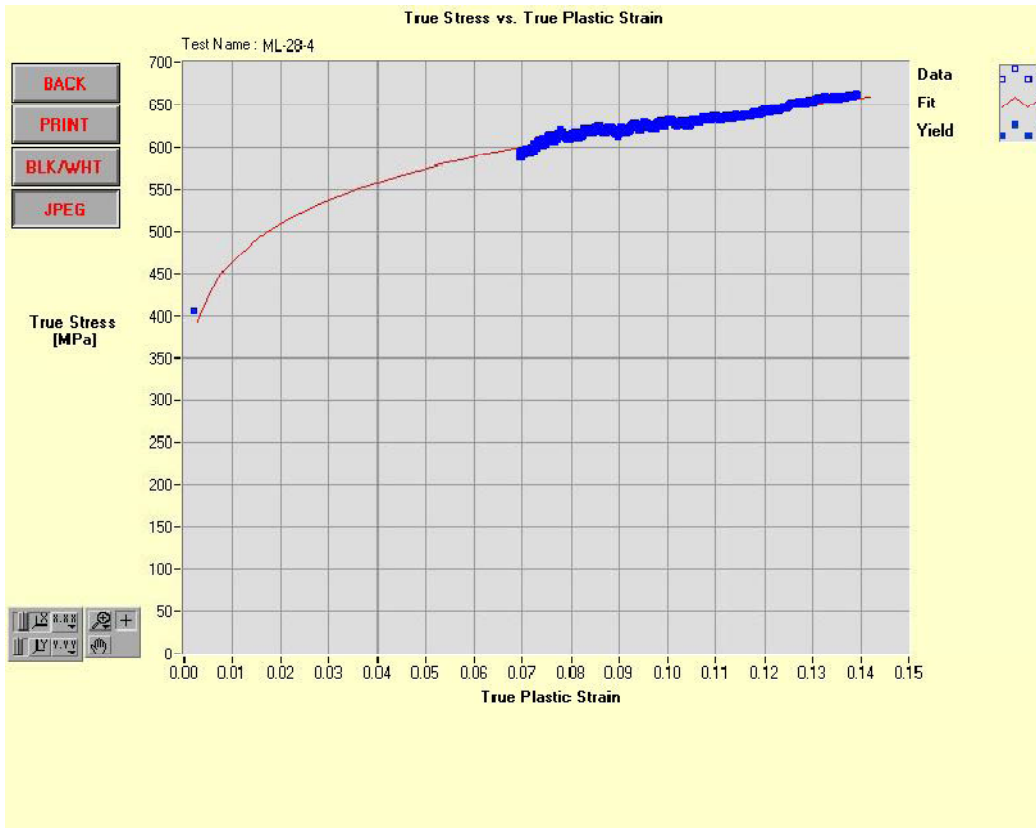


Fig. 9 True-Stress/True-Strain Plot.

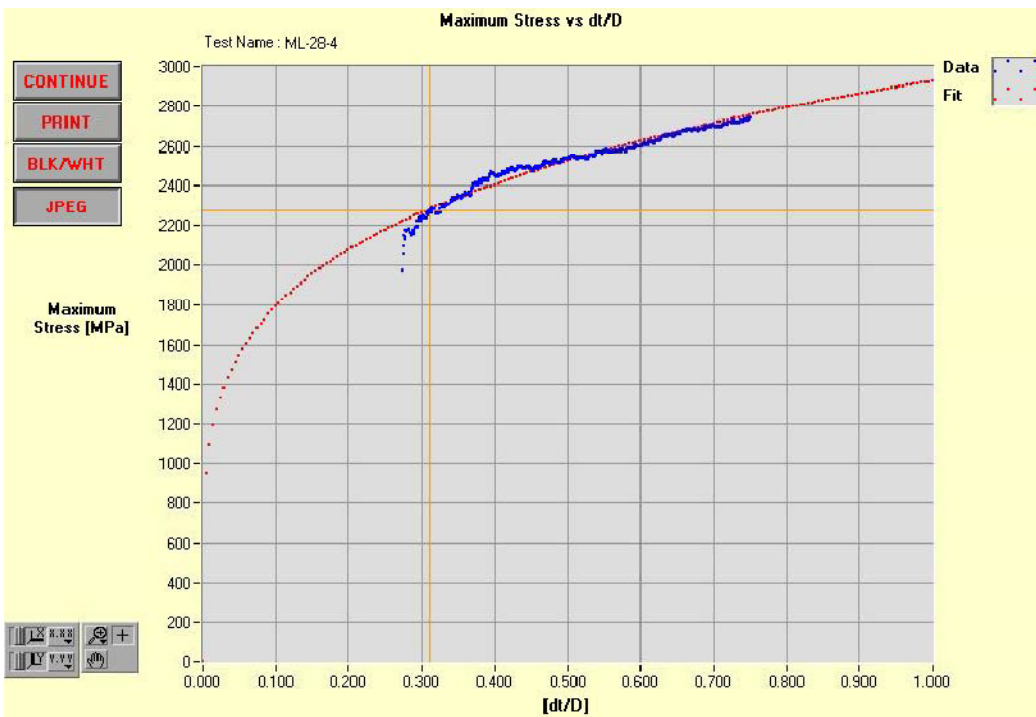


Fig. 10 The Maximum Stress versus Normalized Indentation Depth for Test “ML-28-4” which was Conducted at -33°C (-28°F) on Sample ML.

Triplicate ABI tests were conducted at room temperature on the same pipe steel sample, and the fracture toughness values were calculated from the indentation load-depth data using the critical fracture strain model instead of using the critical fracture stress model that was used earlier for analyzing ABI tests at low test temperatures. The critical-strain (empirically determined) for this new analysis was 0.14 (14%). This new method produced slightly conservative fracture toughness values and the reference temperature value determined from the room temperature ABI tests was -19°C (slightly higher than the -24°C value determined from low-temperature ABI tests). It should be noted that the ABI tests at room temperature [22°C (72°F)] did meet the ASTM requirement for applying the Weibull statistical master curve fitting since they were within the $\pm 50^{\circ}\text{C}$ of the reference temperature for this pipeline material. The new critical fracture strain method analyzing the ABI test data at room temperature was also applied to three pressure-vessel steel materials (Plate 02, and Welds 72W and 73W shown earlier in Fig. 4), and the reference temperatures were also conservative as compared to those from destructive fracture toughness and from ABI tests at low test temperatures.

In order to obtain median dynamic fracture toughness (K_{Id}) values as a function of temperature, the ASTM Standard E1921-97 equation of the static fracture toughness (K_{Jc}) master curve (Reference 12) can be used provided that the reference temperature be shifted to a higher value by the amount of 78°C (140°F). It is well known that the dynamic fracture toughness curve is shifted to the right hand-side of the static fracture toughness curve by a temperature shift value depending on the room-temperature yield strength of the ferritic steel material.

The median dynamic fracture toughness (K_{Id}) can be calculated from the following equation:

$$K_{Id}(med) = 30 + 70e^{0.019(T-[T_0+T_{shift}])} \quad \text{MPa}\sqrt{\text{m}} \quad (7)$$

Where T is the test temperature in $^{\circ}\text{C}$ and T_0 is the reference temperature when $K_{Jc} = 100 \text{ MPa}\sqrt{\text{m}}$.

The T_0 value, determined from the ABI tests at low test-temperatures, to be used in the above equation is -24°C . The T_{shift} of 78°C (140°F) was determined from the Barsom correlation [Ref. 13] and using the average yield strength of 50 ksi that was measured from multiple ABI tests at room temperature. The Barsom correlation is given by:

$$T_{shift} (^{\circ}\text{F}) = 215 - 1.5\sigma_{ys}(ksi) \quad \text{for } 36 \text{ ksi} < \sigma_{ys} < 140 \text{ ksi} \quad (8)$$

where σ_{ys} is the room-temperature yield strength of the steel material.

The static and dynamic fracture toughness median curves for the pipeline steel are provided in Figure 13.

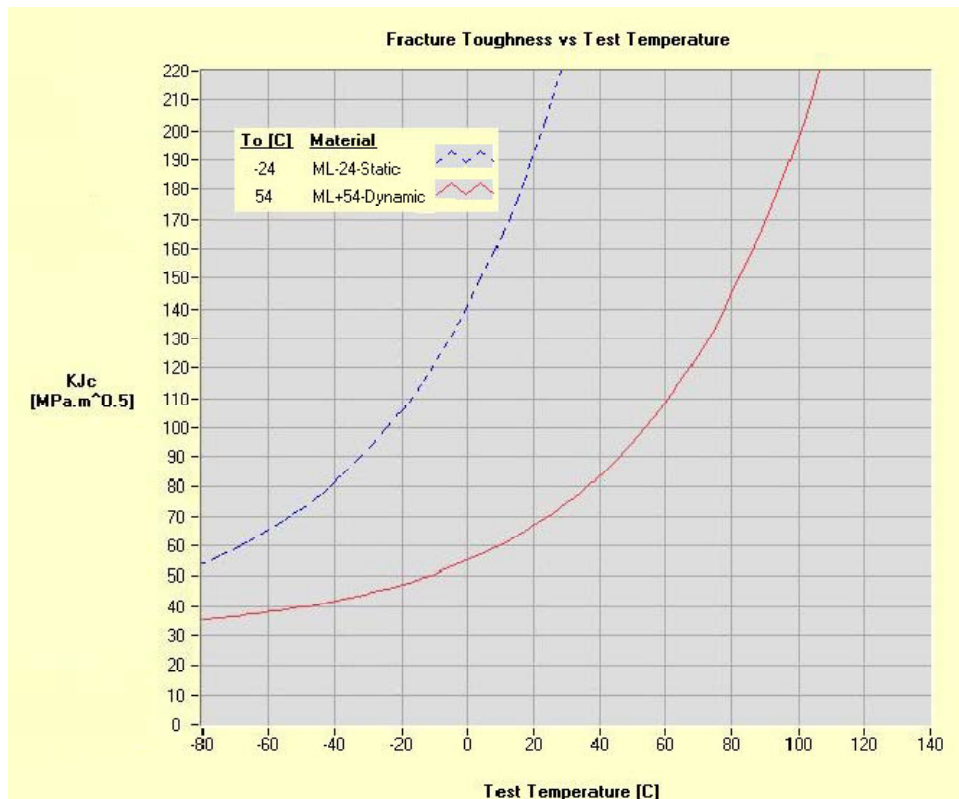


Fig. 13 The Dynamic Median Fracture Toughness Curve is Calculated from the ABI-Determined Static Fracture Toughness Master Curve of the Pipeline Steel Sample by Shifting the Static Curve to the Right by 78°C.

SUMMARY AND CONCLUSIONS

The results presented briefly in this paper and in detail in Refs. [7,10] demonstrate the capabilities of ATC's patented Portable/In-Situ Stress-Strain Microprobe (SSM) system and its Automated Ball Indentation (ABI) test technique to nondestructively measure the yield strength, the stress-strain curve, and fracture toughness of carbon steel materials, from various natural gas pipeline manufacturers, in a reliable and accurate manner on samples and components.

The accuracy, reliability, and easy field applicability of the SSM technology to test pipeline materials with unknown properties have been demonstrated in this work. Reference [10] was reviewed favorably by the US Office of Pipeline Safety (OPS) in December 1999 and the SSM technology is recommended for use by the pipeline industry. The test results of Reference [10] work provide the technical basis for: (1) a pipeline operator to submit a waiver to the OPS of the US Department of Transportation (DOT) to use the ABI test as an alternative to the tensile test, and (2) preparing an Amendment to 49 CFR 192 Appendix B to allow nondestructive ABI testing as an alternative to the destructive and expensive tensile testing to measure the yield strength and the stress-strain curve of steel pipeline with unknown properties. The laboratory version of the SSM system has been in commercial use since 1991 in three continents, and the portable SSM version received a 1996 R&D 100 Award. Furthermore, the miniature SSM-M1000 was introduced by ATC in 1999 to provide even greater portability. Equipped with a portable battery pack and manual magnetic mounts, the SSM-M1000 proved to be a valuable test instrument for the pipeline industry. The use of the SSM system to test pipelines in the field will improve their structural integrity evaluation as well as their operational efficiency (by allowing safe up-rating).

ACKNOWLEDGMENTS

Advanced Technology Corporation (ATC) would like to thank ANR Pipeline Company and Columbia Gas Transmission Corporation for providing several steel pipeline materials (various grades manufactured from 1931 through 1978) to perform the destructive tensile and the nondestructive Automated Ball Indentation (ABI) tests at ATC. The tensile and ABI tests were conducted using ATC's patented Portable/In-Situ Stress-Strain Microprobe (SSM). We extend our sincere thanks to Mr. Ted Clark (Columbia Gas), Mr. Richard Eckert (ANR Pipeline), and Dr. Jude Foulds (Exponent) for attending the miniature tensile testing, ABI blind testing, and the demonstration of the SSM system to test a full-cylindrical pipe section at ATC on June 22 and 23, 1999. The continued encouragement of Mr. Gopala Vinjamuri (Office of Pipeline Safety, US DOT) and Dr. John H. Smith (retired from the Metallurgy Division, National Institute of Standards and Technology, Gaithersburg, MD) during this work is greatly appreciated. Major funding of the ABI-measured fracture toughness development was provided by the US Department of Energy.

REFERENCES

- [1] Haggag, F. M., "Field Indentation Microprobe for Structural Integrity Evaluation," U.S. Patent No. 4,852,397, 1989.
- [2] Haggag, F. M., "In-Situ Measurements of Mechanical Properties Using Novel Automated Ball Indentation System," *ASTM STP 1204*, 1993, pp. 27-44.
- [3] Haggag, F. M., et al., "Use of Portable/In Situ Stress-Strain Microprobe System to Measure Stress-Strain Behavior and Damage in Metallic Materials and Structures," *ASTM STP 1318*, 1997, pp. 85-98.
- [4] Haggag, F. M. et al., "Structural Integrity Evaluation Based on an Innovative Field Indentation Microprobe," *ASME PVP-Vol. 170*, 1989, pp. 101-107.
- [5] Druce, S. G., et al., "The Use of Miniature Specimen Techniques for the Assessment of Material Condition," *ASME PVP-Vol. 252*, 1993, pp. 58-59.
- [6] Byun, T. S., et al., "Measurement of Through-the-Thickness Variations of Mechanical Properties in SA508 Gr.3 Pressure Vessel Steels Using Ball Indentation Test Technique," *International Journal of Pressure Vessels and Piping*, 74, 1997, pp. 231-238.
- [7] Haggag, F. M., "Nondestructive and Localized Measurements of Stress-Strain Curves and Fracture Toughness of Ferritic Steels at Various Temperatures Using Innovative Stress-Strain Microprobe Technology," Report No. DOE/ER/82115-2, 1999.
- [8] Haggag, Fahmy M., "In-Situ Nondestructive Measurements of Key Mechanical Properties of Oil and Gas Pipelines," *ASME PVP-Vol. 429*, 2001, pp. 99-104.
- [9] Byun, T. S., et al., "A Theoretical Model for Determination of Fracture Toughness of Reactor Pressure Vessel Steels in the Transition Region from Automated Ball Indentation Test," *Journal of Nuclear Materials*, 252, 1998, pp. 187-194.
- [10] Haggag, F. M., "Nondestructive Determination of Yield Strength and Stress-Strain Curves of In-Service Transmission Pipelines Using Innovative Stress-Strain Microprobe Technology," Report No. ATC/DOT/990901, 1999.
- [11] Haggag, F. M., "Effects of Irradiation Temperature on Embrittlement of Nuclear Pressure Vessel Steels," *ASTM STP 1175*, 1993, pp. 172-185.
- [12] ASTM Standard E1921-97, "Standard Test Method for Determination of Reference Temperature, T_0 , for Ferritic Steels in the Transition Range," *Annual Book of ASTM Standards*, Vol 03.01.
- [13] Rolfe, Stanley T. and Barsom, John M., *Fracture and Fatigue Control in Structures: Applications of Fracture Mechanics*, Prentice-Hall, Inc., Englewood Cliffs, New Jersey, 1977, p. 129.

VITA

ROBERT L. BRIDGES

Personal Data: Date of Birth: July 15, 1955
 Place of Birth: Knoxville, Tennessee
 Marital Status: Married

Education: Public Schools, Knox County, Tennessee
 Associate Engineering Technician, State Technical Institute of
 Knoxville, Tennessee 1981
 B.A. Engineering Technology, East Tennessee State
 University, Johnson City, Tennessee 2005
 M.A. Engineering Technology, East Tennessee State
 University, Johnson City, Tennessee 2010

Professional Experience: Staff Metallurgical Engineer, Y-12 National Security
 Complex, 1987 – Present

Professional Societies: American Society for Testing and Materials since 2003
 American Society of Metals since 1995

Publications: Bridges, Robert L., Carpenter, Donald A. (2008). “Surface
 Preparation of Uranium by Ion Milling.” *Microscopy Today*.
 The Microscopy Society of America, pp. 28 – 31.
 Czuchry, A., Bridges, R. Parker, M. (2010). “Achieving
 Organizational Sustainability: An Engineering Management
 Challenge or Opportunity?” *American Society for
 Engineering Education*. AC 2010-60

Honors and Awards: Department of Energy award of excellence: 2007, 2005, 2000,
 1999, 1993, and 1989.
 Technical Achievement award: 1993, and 1991.

Patent: U. S. Patent No. 6,264,880 IL-9976A, “Manifold Free Multi
 Sheet Superplastic Forming”, 2001